Photosynthetic Adaptation to Length of Day Is Dependent on *S*-Sulfocysteine Synthase Activity in the Thylakoid Lumen[1][W]

María Ángeles Bermúdez, Jeroni Galmés, Inmaculada Moreno, Philip M. Mullineaux, Cecilia Gotor, and Luis C. Romero*

Instituto de Bioquímica Vegetal y Fotosíntesis, Consejo Superior de Investigaciones Científicas y Universidad de Sevilla, 41092 Seville, Spain (M.Á.B., I.M., C.G., L.C.R.); Grup de Recerca en Biologia de les Plantes en Condicions Mediterrànies, Universitat de les Illes Balears, 07122 Palma, Spain (J.G.); and School of Biological Sciences, University of Essex, Colchester CO4 3SQ, United Kingdom (P.M.M.)

Arabidopsis (*Arabidopsis thaliana*) chloroplasts contain two *O*-acetyl-serine(thiol)lyase (OASTL) homologs, OAS-B, which is an authentic OASTL, and CS26, which has *S*-sulfocysteine synthase activity. In contrast with OAS-B, the loss of CS26 function resulted in dramatic phenotypic changes, which were dependent on the light treatment. We have performed a detailed characterization of the photosynthetic and chlorophyll fluorescence parameters in *cs26* plants compared with those of wild-type plants under short-day growth conditions (SD) and long-day growth conditions (LD). Under LD, the photosynthetic characterization, which was based on substomatal CO_2 concentrations and CO_2 concentration in the chloroplast curves, revealed significant reductions in most of the photosynthetic parameters for *cs26*, which were unchanged under SD. These parameters included net CO_2 assimilation rate, mesophyll conductance, and mitochondrial respiration at darkness. The analysis also showed that *cs26* under LD required more absorbed quanta per driven electron flux and fixed CO_2. The nonphotochemical quenching values suggested that in *cs26* plants, the excess electrons that are not used in photochemical reactions may form reactive oxygen species. A photoinhibitory effect was confirmed by the background fluorescence signal values under LD and SD, which were higher in young leaves compared with mature ones under SD. To hypothesize the role of CS26 in relation to the photosynthetic machinery, we addressed its location inside of the chloroplast. The activity determination and localization analyses that were performed using immunoblotting indicated the presence of an active CS26 enzyme exclusively in the thylakoid lumen. This finding was reinforced by the observation of marked alterations in many lumenal proteins in the *cs26* mutant compared with the wild type.

In plants, Cys biosynthesis is accomplished by the sequential reaction of two enzymes, serine acetyltransferase (SAT), which catalyzes the synthesis of the intermediary product *O*-acetyl-serine (OAS) from acetyl-CoA and Ser, and *O*-acetyl-serine(thiol)lyase (OASTL), which incorporates the sulfide that is derived from the assimilatory reduction of sulfate to OAS, producing Cys. Both enzymes interact to form the heterooligomeric Cys synthase complex, which was first described in bacteria and is now extensively studied in plants (Droux et al., 1998; Wirtz and Hell, 2006). Plant cells contain different SAT and OASTL enzymes that are localized to the cytosol, plastids, and mitochondria, resulting in a complex variety of isoforms and distinct subcellular Cys pools. Arabidopsis (*Arabidopsis thaliana*) contains five different *SAT* genes (Howarth et al., 2003) and nine *OASTL* genes (Wirtz et al., 2004).

Arabidopsis chloroplasts contain two OASTL homologs that are encoded by the *O-ACETYLSERINE (THIOL) LYASE B* (*OAS-B*) (At2g43750) and *CYSTEINE SYNTHASE26* (*CS26*) (At3g03630) genes. At the transcriptional level, *OAS-B* is the most abundant OASTL transcript, and its encoded protein is considered to be an authentic OASTL because of its ability to interact with SAT (Gilbert et al., 1996; Droux et al., 1998; Kidner et al., 2000; Kim et al., 2007). Our group recently investigated *CS26* and clearly demonstrated that the minor chloroplastic OASTL isoform that is encoded by the *CS26* gene from Arabidopsis has *S*-sulfocysteine synthase (SSCS) activity (Bermúdez et al., 2010); to our knowledge, that is the first report of this activity in plants. The CS26 protein is predicted to be localized within the chloroplast on the basis of its N-terminal signal peptide, although this has not yet been demonstrated; however, the predicted amino acid sequence comparison revealed that CS26 contains an extension at the C terminus of the chloroplast transit peptide (cTP) in contrast with OAS-B. The biochemical comparison of the *oas-b* and *cs26* null mutants demonstrated that the *cs26* mutation had no effect on OASTL activity levels,

whereas the *oas-b* mutant had significantly less OASTL activity (Watanabe et al., 2008; Bermúdez et al., 2010). In addition, the loss of CS26 function resulted in dramatic phenotypic changes, which were dependent on the prevailing light treatment. The *cs26* mutant exhibited reduced chlorophyll concentrations and photosynthetic activity, showing elevated glutathione levels, and accumulated reactive oxygen species (ROS) under long-day growth conditions (LD). Although the function of CS26 has not yet been established, *CS26* has been identified as one of the target genes of the long-term response signaling pathway, which is regulated to compensate for the lack of long-term response signaling (Pesaresi et al., 2009).

During optimal photosynthetic conditions, light energy is harvested and channeled into the two reaction centers of PSI and PSII, where charge separation occurs and electrons are passed linearly along the electron transport chain leading to ATP and NADPH production for CO_2 fixation into organic compounds. Under constant moderate light conditions, the efficiency of the energy conversion is high as a result of photochemical reactions. Fluctuations in light intensity, temperature, or water availability may contribute to the overexcitation of PSII, and photoprotective mechanisms are subsequently activated to prevent damage that either involves detoxification of the ROS (Asada, 1999) or the prevention of their formation by the dissipation of excess excited states into heat. The failure to dissipate excitation energy results in the overreduction of the photosynthetic chain components that direct linear electron flux from water to NADPH (Baker, 2008). A portion of the absorbed light energy is dissipated as heat in the light-harvesting complexes of PSII through nonphotochemical quenching (NPQ; Horton et al., 1996; Müller et al., 2001). The additional dissipation of excitation energy is also achieved by photochemical quenching through the reduction of molecular oxygen at PSI via the Mehler reaction and photorespiration (Asada, 1999; Douce and Neuburger, 1999), of which both processes produce ROS. In light-stressed plants, the damaged chloroplasts initiate retrograde signaling to the nucleus (Pogson et al., 2008) to down-regulate the expression of photosynthetic genes and up-regulate stress defense genes to mitigate oxidative stress (Koussevitzky et al., 2007; Mühlenbock et al., 2008).

The aims of this work were to reveal the subcellular localization of CS26 inside the chloroplast and to characterize the photosynthetic limitations that are due to the *CS26* mutation in Arabidopsis under different light treatments.

RESULTS

Leaf Morphology of the *cs26* Mutant Was Affected by Light Conditions

When the leaf phenotypic traits of the *cs26* mutant line were compared with those of the wild type, no significant differences were reported under short-day growth conditions (SD), and similar leaf areas and leaf

mass areas (LMA) were observed (Fig. 1). However, when the plants were grown under LD, both the leaf areas and LMA were reduced by 26% in the *cs26* mutant compared with the wild type, suggesting that the leaves of *cs26* were thinner and/or less dense. Nonvisible changes in leaf morphology were observed in the wild type when comparing the plants that were grown under the two photoperiods (Fig. 1).

Photosynthetic Parameters Were Reduced in the *cs26* Mutant Under Long-Day Conditions Compared with the Wild Type

At saturating light conditions (1,000 μmol m^{-2} s^{-1}) and ambient CO_2 concentrations, nonsignificant differences ($P < 0.05$) were observed between the *cs26* mutant and the wild type under SD for most of the photosynthetic parameters, including net CO_2 assimilation rate (A_N), stomatal conductance (g_s), intrinsic water use efficiency (A_N/g_s), mesophyll conductance (g_m), mitochondrial respiration at darkness (R_{dark}) and stomatal conductance at darkness ($g_{s,dark}$; Table I). At LD, A_N was more severely reduced in the *cs26* mutant than at SD (from 11.1 to 1.9 μmol m^{-2} s^{-1}), while in the wild type, the A_N value at LD decreased at a lower degree compared with that at SD (from 11.6 to 8.3 μmol m^{-2} s^{-1}). However, the g_s values did not significantly differ when comparing plants that were grown under SD and LD for either of the two genotypes. As a result, A_N/g_s was lower under LD than SD in both lines, but stronger photoperiod effects were

C	LMA (gm^{-2})	
	wild-type	*cs26*
Long-day	10.2 ±1.2	7.5 ±0.5*
Short-day	9.8 ±1.5	10.8 ±1.1[†]
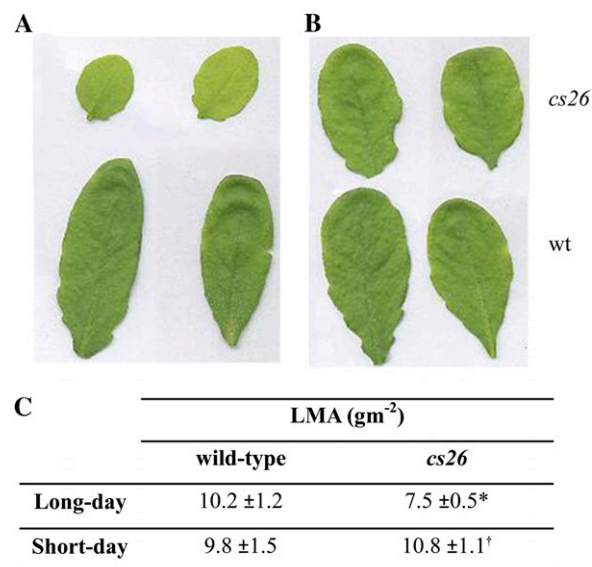
Figure 1. Phenotypic characterization of wild-type (wt) and mutant *cs26* leaves under the two photoperiods. A, Leaves from plants that were grown for 3 weeks under LD. B, Leaves from plants that were grown for 5 weeks under SD. C, LMA. Values are means ± SD ($n = 5$). *Significant difference at $P < 0.05$ between the wild type and *cs26* under a given photoperiod. [†]Significant difference at $P < 0.05$ between plants of the same genotype grown under the two photoperiods.

observed in *cs26* (Table I). The capacities of the leaf mesophyll to transfer CO_2 from the substomatal cavities to the sites of carboxylation (g_m) were similar between the two lines under SD, but under LD, g_m was severely depressed in *cs26*, while it was stimulated in the wild type. All of these factors affected the CO_2 concentration in the chloroplast (C_c), leading to higher values in both lines for the plants that were grown under LD compared with SD. Under SD, no significant differences were observed between the lines with regard to the R_{dark} and $g_{s,dark}$ values, but under LD, the *cs26* mutant showed increased R_{dark} compared with the wild type (Table I).

Under SD, the parameters that were derived from the A_N-C_i (for substomatal CO_2 concentrations) curves were similar between the wild type and *cs26* (Fig. 2A). However, when the two lines were grown under LD, *cs26* presented lower A_N values for any given C_i, a lower initial slope, and a higher CO_2 compensation point on a C_i basis (Fig. 2B). When the A_N-C_i curves were transformed into A_N-C_c curves, a unique difference was revealed between the genotypes under SD; the maximum velocity of carboxylation ($V_{c,max}$) was significantly lower in *cs26* as a result of the slightly lower g_m values in the wild type (Table I; Fig. 2C). Under LD, the differences in the A_N-C_i curves were maintained, with a lower $V_{c,max}$ (37%) and higher CO_2 compensation point on a C_c basis (133%) for *cs26* compared with the wild type (Table I; Fig. 2D). Maximum capacity for electron transport rate (J_{max}) was less affected, yet it was 65% lower in the *cs26* under LD and showed no differences under SD. However, the $J_{max}/V_{c,max}$ ratio stayed almost constant, being slightly higher for the *cs26* SD plants because of the lower $V_{c,max}$ value for *cs26* under this condition (Table I).

A complemented *cs26*:P35S-CS26 line, which expressed the *CS26* gene at levels comparable to the wild type, rescued all the photosynthetic parameters of mutant plants grown under LD to wild-type values (Supplemental Table S1).

The decrease in $V_{c,max}$ may be due to the lower concentration and/or activation of Rubisco. Under SD, no significant differences in the concentrations of Rubisco and total soluble protein were observed between genotypes, but under LD, the *cs26* plants presented 30% of the Rubisco concentration that was observed in the wild type (Table II). Remarkably, such a decrease in Rubisco concentration under LD was not completely driven by a decrease in the concentration of total soluble protein; the ratio of Rubisco to total soluble protein was 63% lower in *cs26* than in the wild type.

The response of A_N and the rate of linear electron transport (J) to increasing light intensities differed between the lines when they were grown under LD, with *cs26* showing lower values for any given photosynthetic active radiation (PAR) intensity (Fig. 3, A and B). At full light-saturating intensities, the corrected J averaged 48.1 and 12.9 μmol e$^-$ m^{-2} s^{-1} for the wild type and the *cs26* line, respectively (Table III). The light intensity at which the A_N-PAR curve showed the inflection point for *cs26* was nearly half that of the wild type because of the presence of lower A_N values. Significant differences between the two lines were also observed for the light compensation point (approximately 3-fold in *cs26*), light use efficiency, as determined from the inverse of the quantum yield (45% higher in *cs26*), and absorbed PAR/J (approximately 2-fold in *cs26*), indicating that the *cs26* line required more absorbed quanta per driven electron flux and fixed CO_2 (Table III). As expected, under these conditions, the A_N values were similar to those obtained from the A_N-C_i curves at a CO_2 concentration (C_a) of 400 μmol mol^{-1}; therefore, the *cs26* plants were less efficient at converting electrons into assimilated CO_2 molecules (i.e. higher J/A_G ratios, where A_G is gross CO_2 assimilation rate). In fact, at full saturating light, the J/A_G ratio for the mutant

Table I. *Photosynthetic characterization of wild-type and cs26 plants grown under LD and SD*

Values represent means ± SD ($n = 6$). A_N, g_s, A_N/g_s, g_m, g_m/g_s, and C_c were obtained from steady-state measurements at a PAR of 1,000 μmol m^{-2} s^{-1} and C_a of 400 μmol mol^{-1}. The g_m and C_c values were estimated according to the variable J method and used to convert the A_N-C_i curves into A_N-C_c. Γ_{Cc}, $V_{c,max}$, and J_{max} were taken from the A_N-C_c curves. R_{dark} and $g_{s,dark}$ were obtained from measurements at darkness and a C_a of 400 μmol mol^{-1}.

Parameter	LD		SD	
	Wild Type	cs26	Wild Type	cs26
A_N (μmol CO_2 m^{-2} s^{-1})	8.3 ± 0.3	1.9 ± 0.3[a]	11.6 ± 0.9[b]	11.1 ± 0.5[b]
g_s (mol water m^{-2} s^{-1})	0.20 ± 0.07	0.18 ± 0.08	0.17 ± 0.01	0.18 ± 0.02
A_N/g_s (μmol CO_2 mol^{-1} water)	41.4 ± 0.8	10.4 ± 0.5[a]	68.1 ± 4.1[b]	61.8 ± 6.2[b]
g_m (mol CO_2 m^{-2} s^{-1})	0.42 ± 0.09	0.01 ± 0.01[a]	0.10 ± 0.03[b]	0.14 ± 0.05[b]
g_m/g_s (mol CO_2 mol^{-1} water)	2.05 ± 0.06	0.05 ± 0.01[a]	0.58 ± 0.12[b]	0.78 ± 0.14[b]
C_c (μmol CO_2 mol^{-1} air)	374 ± 34	340 ± 20	230 ± 23[b]	295 ± 10[a,b]
R_{dark} (μmol CO_2 m^{-2} s^{-1})	−1.01 ± 0.25	−1.77 ± 0.33[a]	−0.56 ± 0.29[b]	−0.57 ± 0.10[b]
$g_{s,dark}$ (mol water m^{-2} s^{-1})	0.27 ± 0.13	0.28 ± 0.06	0.05 ± 0.01[b]	0.07 ± 0.02[b]
$V_{c,max}$ (μmol CO_2 m^{-2} s^{-1})	24.6 ± 2.6	9.0 ± 2.3[a]	41.0 ± 5.0[b]	31.6 ± 1.4[a,b]
J_{max} (μmol CO_2 m^{-2} s^{-1})	48.6 ± 2.5	17.3 ± 5.1[a]	80.7 ± 12.1[b]	74.9 ± 4.7[b]
$J_{max}/V_{c,max}$	2.0 ± 0.2	1.9 ± 0.4	2.0 ± 0.1	2.4 ± 0.1[a,b]
Γ_{Cc} (μmol CO_2 mol^{-1} air)	51.0 ± 2.6	119.0 ± 10.0[a]	42.8 ± 1.6[b]	42.0 ± 1.6[b]

[a]Significant differences between the *cs26* mutant and the wild type grown under the same photoperiod ($P < 0.05$). [b]Significant differences between LD- and SD-grown plants for the same genotype ($P < 0.05$).
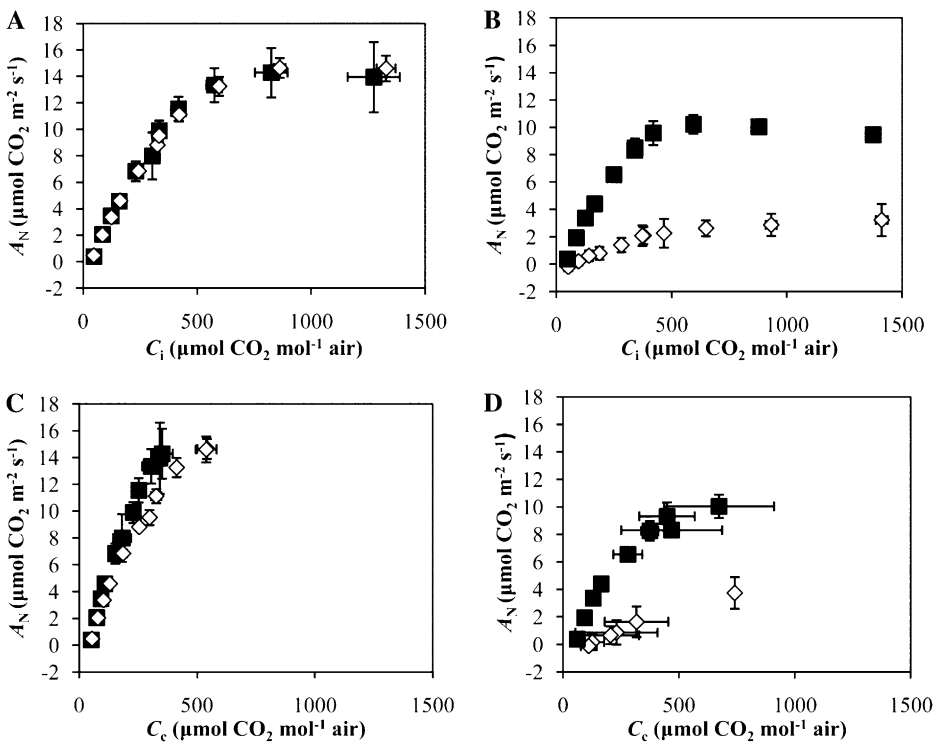
Figure 2. Photosynthetic rates for wild-type and *cs26* plants. Determination of the A_N at varying substomatal C_i or C_c values was performed for wild-type (black squares) and *cs26* (white diamonds) plants of Arabidopsis under SD (A and C) and LD (B and D). The values are averages ± SE of six replicates per genotype, photoperiod, and CO_2 concentration.

was 45% higher than that for the wild type (Table III). A closer inspection revealed that at the growth light intensity (approximately 100 μmol m^{-2} s^{-1}), J/A_G displayed the maximum difference between *cs26* and the wild type (approximately 3.4-fold in *cs26*). The average values for NPQ at full light saturation were also statistically different (approximately 2-fold in *cs26*; Table III).

The complemented *cs26*:P35S-CS26 line also rescued all the photosynthetic parameters derived from light-response curves of mutant plants grown under LD to wild-type values (Supplemental Table S2).

Chlorophyll Fluorescence Parameters Showed Differences in *cs26* Plants Compared with Wild-Type Plants Depending on Light Intensity and Growth Stage

In the wild-type leaves, the maximum quantum efficiency of PSII photochemistry (F_v/F_m) was approximately 0.8 for the plants that had been grown under both

SD and LD (Fig. 4, A and B). In contrast, a reduction in F_v/F_m was observed in the *cs26* leaves that had been grown under both photoperiods compared with those of the wild type, with stronger reductions under LD, indicating a severe defect in PSII. Under SD, the younger rosette leaves from *cs26* presented lower F_v/F_m values when compared with the mature leaves (Fig. 4A), suggesting the presence of PSII photoinhibition in the *cs26* mutant line. The high levels of background fluorescence signal (F_o) in the *cs26* mutant under LD (52 ± 11 in *cs26* compared with 11 ± 1 in the wild type) are indicative of lower concentrations of coupled chlorophylls and/or damage to the photosynthetic apparatus. Moreover, the overall F_o value of the *cs26* plants under SD was also higher (62 ± 5 in *cs26* compared with 31 ± 1 in the wild type); however, an increase was also observed in F_o in the young leaves compared with the mature ones (89 ± 2 versus 58 ± 8), verifying the presence of altered photochemistry in the younger leaves. Under LD, it was also

Table II. *Total soluble protein and Rubisco concentrations*

Leaf extracts from wild-type and *cs26* plants grown under the two photoperiods were obtained. Total soluble protein was determined by the method of Bradford (1976), and the Rubisco concentrations were determined by SDS-PAGE titration as described in "Materials and Methods." Values are averages ± SE (*n* = 3).

Plant	Total Soluble Protein		Rubisco		Rubisco/Total Soluble Protein	
	LD	SD	LD	SD	LD	SD
			$\mu g \, \mu L^{-1}$			
Wild type	4.00 ± 0.28	4.17 ± 0.02	1.06 ± 0.05	0.85 ± 0.02[b]	0.27 ± 0.02	0.20 ± 0.01[b]
cs26	3.10 ± 0.07[a]	3.87 ± 0.12[b]	0.31 ± 0.01[a]	0.72 ± 0.13[b]	0.10 ± 0.01[a]	0.18 ± 0.03[b]

[a]Significant differences between wild-type and *cs26* data within the same photoperiod (*P* < 0.05). [b]Significant differences between LD- and SD-grown plants within the same genotype (*P* < 0.05).
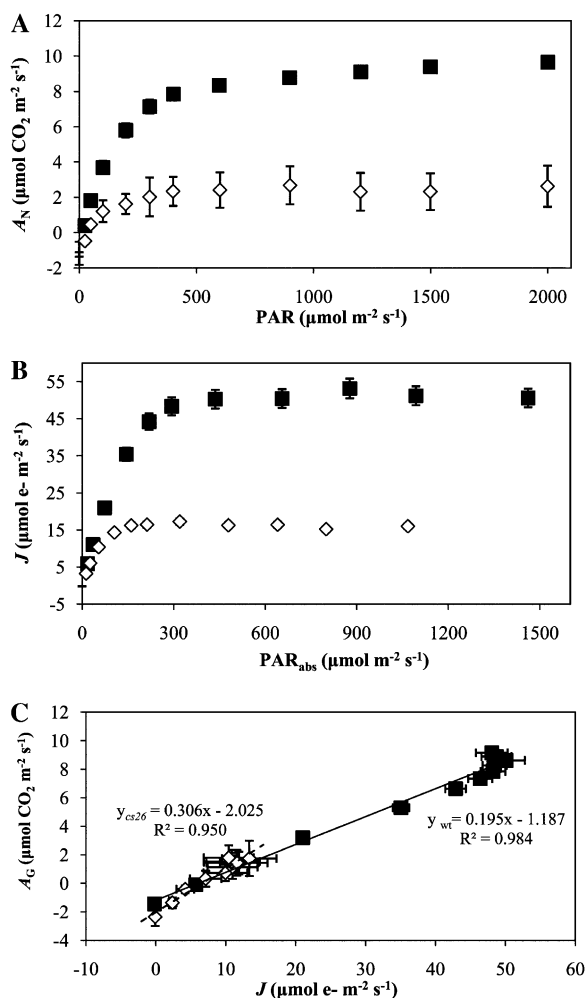
Figure 3. Light-response curves in wild type (black squares) and *cs26* (white diamonds) under LD. A, The response of A_N to PAR. B, The response of J to absorbed PAR (PAR$_{abs}$). C, The relationship between J and A_G, A_G being the sum of A_N and R_L. PAR$_{abs}$ was obtained by correcting the incoming PAR intensities with the leaf absorbance, which was taken from the product of $\alpha \cdot \beta$, considering β as constant and equal to 0.5. In C, the regression lines for the wild type (solid lines) and *cs26* (dashed lines) are shown. The values are averages ± SD for six replicates per genotype and photoperiod.

observed that the level of minimal chlorophyll fluorescence from light-adapted leaves was actually reduced by 38% (32 ± 3) compared with F_o in the *cs26* plants, which is unusual. At growth light intensities, *cs26* showed higher NPQ values under both photoperiods compared with the wild type (Fig. 4, C and D). Following exposure to 800 μmol m^{-2} s^{-1}, the NPQ increased in both genotypes, indicating the presence of increased heat dissipation from PSII (Fig. 4, E and F). In mutant plants under SD, the NPQ values were lower in the younger leaves compared with the mature ones irrespective of the actinic light intensity (Fig. 4, C and E). These results are in agreement with the expression of the *CS26* gene in different tissues and developmental stages of Arabidopsis, showing the highest transcript accumulation in the

leaves of early-stage plants (stage 1.07) and stems and flowers (stage 6.1, where 10% of flowers to be produced are opened; Fig. 5). The accumulation of the *CS26* transcript decreased during the mature stages, showing the lowest values in the leaves of senescent plants (stage 8.0).

Under all of the studied conditions, the *cs26* plants presented lower values for the PSII operating efficiency (F_q'/F_m') compared with the wild type (Table IV). Similarly, there was a reduction in the maximum efficiency of PSII photochemistry (F_v'/F_m') in the mutant line compared with the wild type (Table IV). These decreases were independent of the photoperiod or the intensity of the actinic light applied, indicating that the PSII reaction centers were probably damaged, because the PSII operating and maximum efficiencies for the reduction of the primary plastoquinone acceptor of PSII were low even under nonsaturating light intensities. Consequently, in all cases with the exception of *cs26* under LD at 150 μmol m^{-2} s^{-1}, the PSII efficiency factor (qP) was lower in *cs26* than in the wild-type plants.

CS26 Protein Location in Chloroplast Fractions

Comparisons of the deduced amino acid sequences of the homologous OASTL proteins that were located in the chloroplasts revealed that CS26 contains a C-terminal extension to the cTP in contrast with the other chloroplast OASTL isoform, OAS-B, suggesting that it may be localized to the thylakoid lumen (Bermúdez et al., 2010). To confirm this observation, we performed a protein-blot analysis of the stromal and thylakoid lumenal fractions using anti-CS26 antibodies that were obtained from purified recombinant proteins. Because of the high sequence homologies of the different OASTLs, anti-CS26 antibodies cross-react and recognize other isoforms, including OAS-B; therefore, for an accurate identification, we performed the protein-blot analysis in the wild type and *oas-b* and *cs26* mutant lines.

Representative images of the stained gel and the protein-blot analysis are shown in Figure 6. Some Coomassie blue-stained bands from the stromal and lumenal fractions were excised and analyzed by matrix-assisted laser-desorption ionization time of flight (MALDI-TOF), and the detected proteins were identified as the stromal and lumenal proteins, respectively, confirming the high purities of the extracts and validating our results (Fig. 6, A and C). In addition, a protein-blot analysis was also performed using anti-stromal Rubisco activase and anti-lumenal PsbO antibodies to detect any cross-contamination between the stromal and lumenal fractions (Supplemental Fig. S1), again confirming the high purities of the protein extracts.

In the stromal fraction, the anti-CS26 antibodies recognized different proteins, some of which were found in the three lines and had molecular masses of over 45 kD; hence, they were considered to be nonspecific. However, a strong band below 37 kD was observed in the wild type and *cs26* that was missing in

Table III. *Photosynthetic parameters derived from light-response curves in wild-type and cs26 plants under LD*

J, *J*/A_G, NPQ, and Absorbed PAR (PAR$_{abs}$)/*J* values were obtained at saturating light intensities (1,000 μE m^{-2} s^{-1}). PAR$_{abs}$ was obtained by correcting the incoming PAR intensities with the leaf absorbance, taken from the $\alpha \cdot \beta$ product and considering β constant and equal to 0.5. The values are averages $\pm$ SE for six replicates per genotype. Asterisks indicate significant differences at $P < 0.05$ between the wild type and the *cs26* mutant line.

Parameter	Wild Type	*cs26*
J (μmol e$^-$ m^{-2} s^{-1})	50.1 $\pm$ 2.7	11.9 $\pm$ 2.7*
Inflection point (μmol m^{-2} s^{-1})	533 $\pm$ 25	234 $\pm$ 56*
Light compensation point (μmol m^{-2} s^{-1})	15.4 $\pm$ 6.6	51.3 $\pm$ 7.2*
1/quantum yield (mol photons mol^{-1} CO$_2$)	16.3 $\pm$ 1.1	23.6 $\pm$ 1.4*
PAR$_{abs}$/*J* (mol photons mol^{-1} e$^-$)	3.5 $\pm$ 0.1	7.8 $\pm$ 0.9*
J/A_G (mol e$^-$ mol^{-1} CO$_2$)	5.8 $\pm$ 0.5	8.3 $\pm$ 0.9*
NPQ	0.9 $\pm$ 0.2	1.9 $\pm$ 0.5*

the *oas-b* mutant (Fig. 6B). The experimental mass of this band was 35.5 kD and matched the estimated mass of the mature OAS-B protein (35.4 kD), which may have been due to a cross-reaction with the antibody. Furthermore, in this fraction, a minor band of 40 kD was observed that was missing in the *cs26* line and matched with the predicted size of the premature CS26 enzyme, which still contains the lumen-targeting transit peptide.

In the lumenal fraction, two bands of different intensities were found in the wild type and *oas-b*, but not in *cs26*, that may correspond with the protein CS26 (Fig. 6D). The higher intensity band was found at 34.8 kD, matching the predictive CS26 mature protein that was calculated by the TargetP and ChloroP programs (www.cbs.dtu.dk), with a mass of 34.1 kD due to the loss of the lumen-targeting transit peptide. The additional minor band at 40 kD that was detected in the stromal fractions of the wild-type and *oas-b* lines was also observed in the lumenal fraction and may match with a nonmature form of the CS26 protein without the chloroplast-targeting transit peptide, or it may be the result of posttranslational modifications of the protein, as already described for other OASTL isoforms, such as N-terminal acetylation (Wirtz et al., 2010) and Tyr nitration (Alvarez et al., 2011).

SSCS activity was also determined in stromal and lumenal extracts from wild-type, *oas-b*, and *cs26* plants that were grown under LD and SD (Fig. 7). Similar results with regard to order of magnitude were obtained in the wild-type and *oas-b* plants, and no activity was detected in the *cs26* plants under either photoperiod. The SSCS activity levels in the stromal fractions were very low compared with the levels that were obtained from the lumenal fractions, which were 3 orders of magnitude greater. These data suggest that the lumen-localized CS26 protein of 34.8 kD is the active form.

Loss of the CS26 Protein Strongly Affects Protein Content of the Thylakoid Lumen

To further characterize the impact of the loss of CS26 on the chloroplast under LD, we performed a proteome analysis of the thylakoid lumen of LD-grown *cs26* mutant and wild-type plants to determine whether there were significant changes at the protein level in this compartment in the absence of the CS26 protein. The resulting two-dimensional (2-D) maps of the lumenal wild-type proteins were highly reproducible and showed very similar protein patterns compared with those that have been reported previously (Kieselbach et al., 1998; Supplemental Fig. S2). Furthermore, almost all of the analyzed proteins in the lumenal fraction were identified as lumen localized (Table V), providing additional validation regarding the purities of the preparations. There were significant differences in the intensities and quantities of the detected proteins in both maps. Despite our strong efforts, we were unable to identify the CS26 protein in the wild-type lumenal fraction. However, we did observe strong alterations in many lumenal proteins of the *cs26* mutant compared with the wild type. The extrinsic subunits of PSII, the PsbP domain protein, HCF136 protein, cyclophilin and FKBP-type peptidyl-prolyl cis-trans-isomerase, Deg1 and D1 processing proteases, and the peripheral thylakoid ATP synthase CF1 α- and β-subunits were all markedly reduced in the null *cs26* mutant, whereas the plastid-lipid-associated protein FBR2 in the thylakoid membrane and plastoglobule was strongly induced in the mutant (Table V). These results suggest that the lack of CS26 protein in the thylakoid lumen greatly affects the stability of many lumenal proteins.

DISCUSSION

Prior to this work, our group established that the phenotypic characteristics of *cs26* mutant plants are dependent on the light treatment. While under SD, *cs26* mutant plants were phenotypically indistinguishable from wild-type plants; when they were grown under LD, the *cs26* mutant plants exhibited reductions in size and green paleness, and these phenotypic traits were even more severe under continuous light, suggesting a possible defect in photosynthesis under LD (Bermúdez et al., 2010). That finding has been confirmed by this study.

Figure 4. Representative whole-rosette chlorophyll fluorescence images. A and B, Images for the F_v/F_m were obtained from wild-type (wt) and *cs26* plants that were grown for 5 weeks under SD (A) and for 3 weeks under LD (B). C to F, Images for NPQ under SD and LD at PPFD of 150 μmol m^{-2} s^{-1} (C and D, respectively) and 800 μmol m^{-2} s^{-1} (E and F, respectively). Color scales for each parameter are shown.
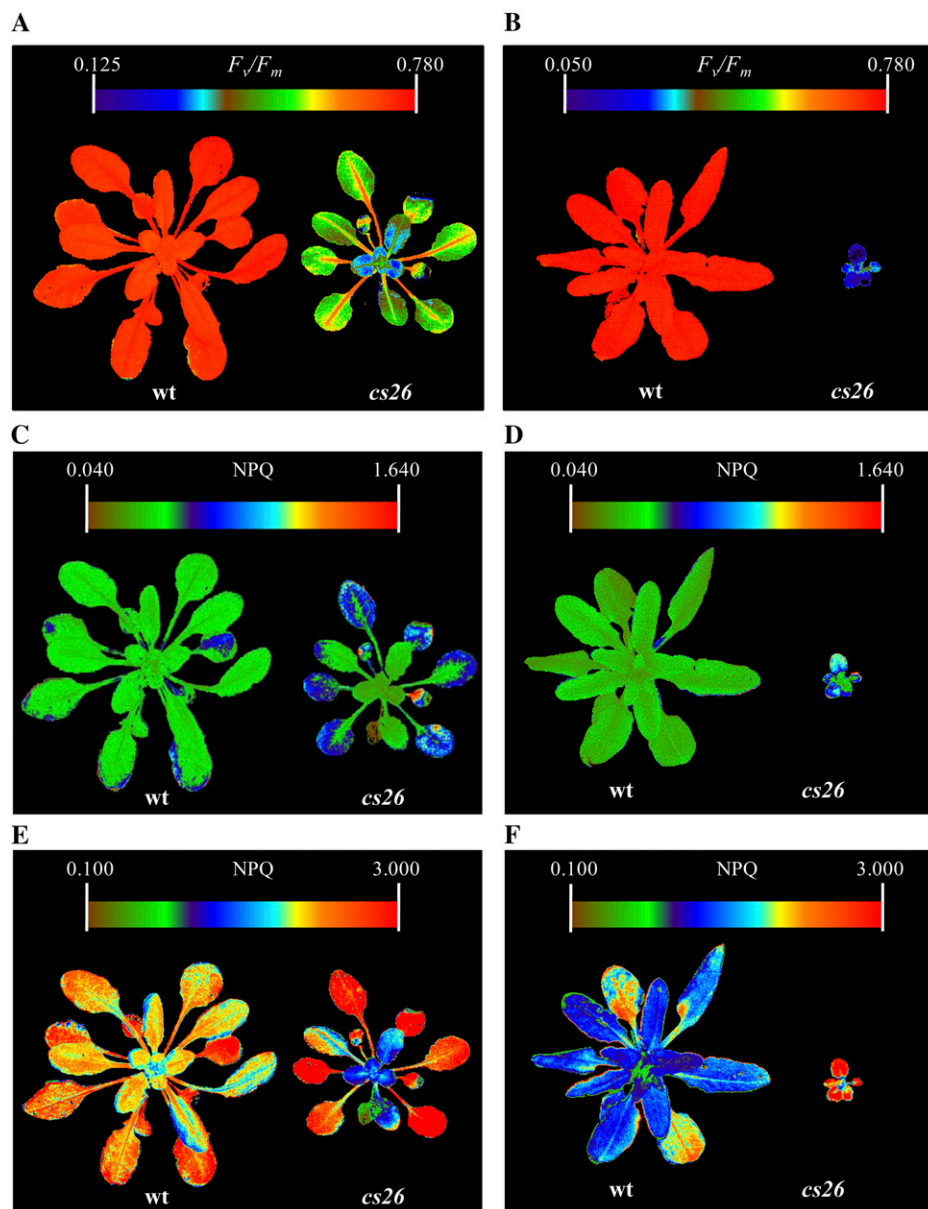
Under LD conditions, the photosynthetic characterization that was based on the C_i and C_c curves revealed significant reductions in most of the photosynthetic parameters in *cs26*, which were restored under SD (Fig. 2; Table I). Among these parameters, the *cs26* mutants under LD displayed reduced photosynthetic capacities, although they maintained open stomata, resulting in lower photosynthetic water use efficiencies. In fact, the lower A_N values in *cs26* under LD were due to biochemical limitations (i.e. decreased $V_{c,max}$) and, particularly, a mesophyll conductance limitation (approximately 65% of A_N limitation). The lower $V_{c,max}$ was partially explained by decreased concentrations of Rubisco (Table II). However, we cannot exclude the possibility that part of the reduction in $V_{c,max}$ was due to lower Rubisco activity through an alteration in the redox regulation of Rubisco activase, which is

necessary for the light modulation of Rubisco (Zhang et al., 2002). It has been shown that g_m depends on leaf morphological characteristics, displaying an inverse correlation with LMA (Flexas et al., 2007a). However, that was not the case in this study, in which decreases in both g_m and LMA were observed (Fig. 1). In other mutant lines with altered redox regulation, increased LMA was observed in LD- compared with SD-grown plants (Lepistö et al., 2009).

Remarkably, the photosynthetic performance of wild-type plants was also affected by the photoperiod under which they were grown, but to lesser degrees than in the *cs26* mutants (Table I). Some previous reports have estimated the g_m for Arabidopsis that is grown under a 12-h-light/12-h-dark photoperiod to be 250 μmol m^{-2} s^{-1}, although g_m values depend upon plant ontogeny (Flexas et al., 2007a). Here, we
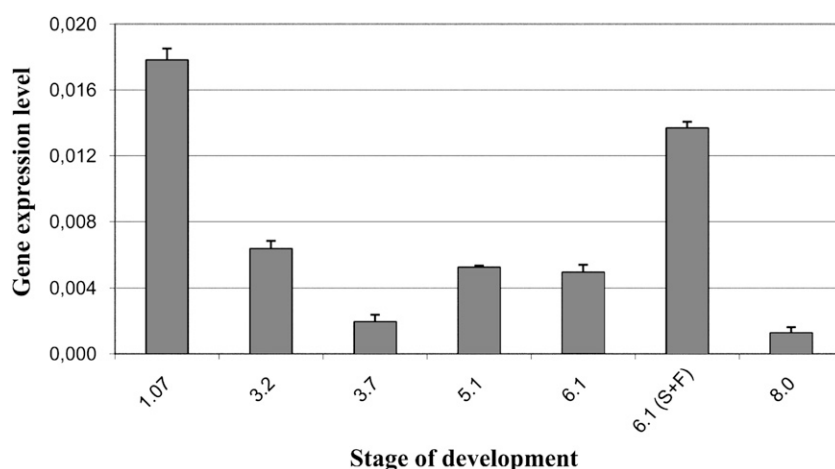
Figure 5. Expression levels of *CS26* in wild-type plants. Real-time reverse transcription-PCR analysis of the expression of the *CS26* gene was performed at different stages in the development of soil-grown wild-type plants. The transcript levels were normalized using the constitutive *UBQ10* gene as an internal control. At each developmental stage, leaves from the rosettes were analyzed, with the exception of stage 6.1, at which the stems and flowers were also analyzed (S+F). Data shown are means ± SD of three independent analyses using RNA that was obtained from different plants that were grown in separate pots at the same time.

obtained similar values in the wild-type plants under SD but higher values under LD. Changes in the g_m following alteration of the spectral quality of light have previously been reported (Loreto et al., 2009), but to our knowledge this is the first report of a significant influence of photoperiod length on the regulation of CO_2 transfer through the leaf mesophyll. The increased g_m in LD wild-type plants did not correlate with changes in LMA, suggesting an up-regulation of biochemical factors that are probably related to carbonic anhydrase or aquaporin functioning. To our knowledge, there are no studies available on the regulation of these proteins corresponding with different photoperiod lengths; however, there is evidence that increasing light intensity also increases aquaporin and carbonic anhydrase activities (Moskvin et al., 2000; Kim and Steudle, 2007).

Further effects of photoperiod length on the leaf carbon balance were observed in both genotypes (Table I). The increased R_{dark} in LD-grown plants is not related to an increased growth demand for energy,

because the plants of both genotypes grew less under LD compared with SD (Bermúdez et al., 2010). Differences between the respiration rates in LD- and SD-grown wild-type plants may be related to the nature of the substrate that supports the respiration, and additionally, light-enhanced dark respiration has been demonstrated in several plant systems (Reddy et al., 1991; Ekelund, 2000; Padmasree et al., 2002). In wild-type plants under LD, carbohydrates are used primarily as respiratory substrates, but under SD, there is a shift at the end of a long night from carbohydrates to organic acids, due to the limited carbon supply from the starch reserves (Zell et al., 2010). Increased dark respiration may also protect photosynthesis from photoinhibition and allow for the dissipation of redox equivalents out of chloroplasts (Saradadevi and Raghavendra, 1992; Singh et al., 1996; Raghavendra and Padmasree, 2003).

The analysis of the response of A_N and J to increasing light intensities revealed that *cs26* plants under LD absorbed less light than the wild-type plants (Fig. 3;

Table IV. *Photosynthetic parameters from light-adapted wild-type and cs26 plants calculated by the chlorophyll fluorescence imaging system*

Measurements were made at two different PPFD levels (150 and 800 μmol m^{-2} s^{-1}). The values shown are averages ± SE of three measurements at each actinic light for three replicates per line.

Parameter and Condition	150 μmol m^{-2} s^{-1}		800 μmol m^{-2} s^{-1}	
	Wild Type	cs26	Wild Type	cs26
LD				
F_v/F_m	0.736 ± 0.006	0.192 ± 0.046[a]	0.736 ± 0.006	0.192 ± 0.046[a]
F_q'/F_m'	0.439 ± 0.024	0.202 ± 0.002[a]	0.314 ± 0.007	0.135 ± 0.001[a]
F_v'/F_m'	0.675 ± 0.002	0.306 ± 0.005[a]	0.529 ± 0.004	0.331 ± 0.021[a]
qP	0.649 ± 0.036	0.611 ± 0.001	0.592 ± 0.015	0.435 ± 0.038[a]
NPQ	0.138 ± 0.008	0.298 ± 0.020[a]	0.620 ± 0.019	0.915 ± 0.051[a]
SD				
F_v/F_m	0.716 ± 0.005	0.488 ± 0.016[a]	0.716 ± 0.005	0.488 ± 0.016[a]
F_q'/F_m'	0.375 ± 0.013[b]	0.286 ± 0.003[a,b]	0.255 ± 0.006[b]	0.182 ± 0.001[a,b]
F_v'/F_m'	0.639 ± 0.007[b]	0.403 ± 0.002[a,b]	0.454 ± 0.004	0.441 ± 0.002[b]
qP	0.587 ± 0.017[b]	0.734 ± 0.001[a,b]	0.577 ± 0.023	0.515 ± 0.006[a,b]
NPQ	0.172 ± 0.017	0.252 ± 0.029[a]	0.879 ± 0.041[b]	1.012 ± 0.020[a,b]

[a]Significant differences between genotypes grown under the same photoperiod ($P < 0.01$). [b]Significant differences between LD- and SD-grown plants within the same genotype ($P < 0.01$).

Figure 6. Localization of CS26 and OAS-B proteins in chloroplast of Arabidopsis. Stroma and lumen preparations from Arabidopsis were isolated from 40 g of leaves of wild-type (wt) and *oas-b* and *cs26* mutant plants that were grown for 5 weeks under SD. In all, 100 μg of stromal or 30 μg of lumenal protein extracts was electrophoresed on 12% acrylamide gels. One replicate was stained with Coomassie blue (A and C), and the second was used for immunoblot analyses using anti-CS26 antibodies (B and D). Proteins identified by MALDI-TOF were as follows: RBCL (Rubisco large subunit), RCA (Rubisco activase), GAP-A (glyceraldehyde 3-phosphate dehydrogenase A subunit), PGK1 (phosphoglycerate kinase1), FBA (Fru-bisP aldolase, class I), FNR [ferredoxin-NADP(H) oxidoreductase], PsbO (oxygen-evolving enhancer), TL29 (ascorbate peroxidase4), DegP1 (DEG protease1), HCF136 (high chlorophyll fluorescence136), and TLP38 (cyclophilin38). Specific bands for the OAS-B and CS26 proteins that were detected by the antibody are shown. MW, Molecular weight markers.
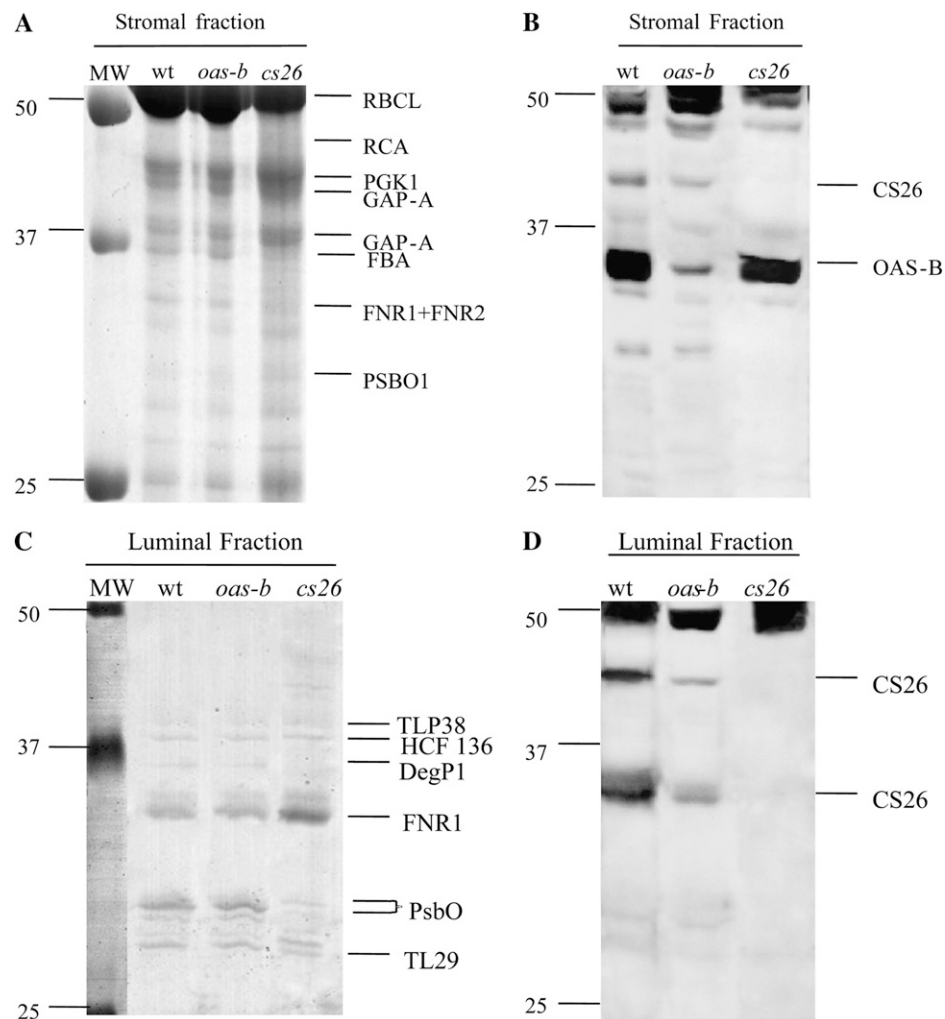

Table III). Additionally, there were lower proportions of absorbed photons being converted to electrons and lower amounts of electrons participating in the carboxylation reaction. The fact that NPQ was not particularly activated in the *cs26* plants under nonsaturating light conditions (Fig. 4, C and D) suggests that the excess electrons that were not used in photochemical reactions may have developed into ROS. In support of this, an increase in the production of ROS was detected by the histochemical analysis, including the superoxide radical anion and hydrogen peroxide, in the *cs26* mutant plants under LD (Bermúdez et al., 2010). R_{dark} showed a greater increase in the LD-grown *cs26* plants, and the transcriptomic data showed a 5.56-fold increase in the mRNA accumulation of a mitochondrial alternative oxidase (AOX; Gene Expression Omnibus repository no. GSE19241). AOX can be induced to decrease the level of ROS, but it is clearly insufficient because *cs26* shows severe growth inhibition in LD (Yoshida et al., 2008; Bermúdez et al., 2010).

A photoinhibition effect was confirmed in the *cs26* mutant according to the F_o values. Additionally, the level of chlorophyll fluorescence after the saturating pulse (F_o') was found to be unusually lower than F_o in the *cs26* plants. Some previous work showed mutants whose fluorescence levels transiently dropped below the F_o level during illumination, similar to the *cs26* mutant. This phenomenon was recently observed in *psbO-1* and *lto1* mutants and mutants of the cytochrome b_{559} subunit of PSII (Murakami et al., 2002; Bondarava et al., 2010; Karamoko et al., 2011). It has been proposed that the PSII pool is partially reduced in the dark in mutants with low PSII activity, which would result in increased F_o levels, suggesting that the cyclic electron flow pathway would have been activated. Thus, it would allow for the mutants to use PSI and cytochrome b_6f to pump protons, thereby synthesizing ATP in the absence of significant levels of linear electron flow as a result of the PSII deficiency.

The lack of *CS26* and photosynthetic defects seems to be associated with developmental stages of growth under SD. Data that were obtained from the *cs26* mutant showed opposite trends with regard to the normal evolution of photosynthetic efficiency during wild-type leaf development (Stessman et al., 2002) and correlated with an accumulation of the *CS26* transcript
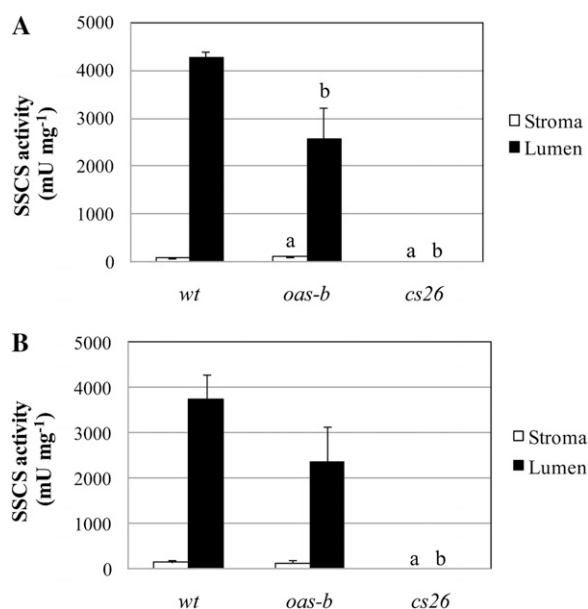
Figure 7. SSCS activity in stromal and lumenal fractions under LD (A) and SD (B). SSCS activity was measured in stromal (white columns) and lumenal (black columns) fraction extracts from the chloroplasts of the wild-type (wt) and *oas-b* and *cs26* mutant lines. Values are means ± SD of three independent determinations. Significant differences between mutants and the wild type in the stromal fraction are indicated by the letter a ($P < 0.05$), and significant differences between mutants and the wild type in the lumenal fractions are indicated by the letter b ($P < 0.05$).

in earlier stages (Fig. 5). Therefore, the loss of *CS26* seems to have a significant impact in early developmental stages.

The dramatic effect of the loss of function of the CS26 protein in the chloroplast suggests that SSCS enzyme activity or the metabolite *S*-sulfocysteine play critical roles in maintaining the photosynthetic machinery. To make a hypothesis regarding the function of this enzyme, it is essential to confirm the subcellular localization of this protein. Prior to this work, a comparison of the amino acid-deduced sequences of several OASTL proteins revealed that CS26 contains an extension at the C terminus of the cTP, in contrast with OAS-B. Using the ChloroP and TargetP cellular localization programs, the cleavage site predictions of OAS-B and CS26 indicated transit peptide lengths of 58 and 84 amino acids, respectively, which correlate with average-sized cTP and the total presequence of lumenal proteins (cTP + the lumenal transit peptide). Lumen-targeting proteins codified by the nuclear genome are synthesized in the cytosol by a bipartite N-terminal transit peptide with two signals in tandem that share a similar structure with prokaryotic sequences that use the secretory/twin-arginine translocase (Tat) systems (Robinson et al., 2001; Gutensohn et al., 2006; Aldridge et al., 2009). The transit peptides are characterized by an N-terminal basic region, a hydrophobic central core, and a polar C-terminal

region ending in an Ala-X-Ala terminal processing site. Proteins that are destined to be transported by the Tat pathway contain a characteristic pair of Arg residues in the N-terminal region of the signal peptide (Aldridge et al., 2009). The extension of the lumen-targeting transit peptide of CS26 is compatible with this structure, possessing a basic N-terminal domain with six Lys residues and one Arg, a hydrophobic central domain with six Pro residues, and a polar C-terminal domain with some Asp residues. Although the lumen transit peptide of CS26 does not have the Ala-X-Ala processing site or the ArgArg residues that are necessary for the Tat transport system, it does possess the LysArg modification that has been described for some proteins that use the Tat system (Peltier et al., 2002).

Massive proteomic analyses did not allow for the identification of the CS26 protein in any previous work, suggesting that it is present at low levels (Zybailov et al., 2008). Activity determination and localization analyses by protein blot supported the idea of the predicted subcellular localization of CS26, showing the presence of the enzyme in both the stromal and lumenal fractions, but it was much more abundant in the latter compartment (Fig. 6). However, its activity was almost exclusive to the thylakoid lumen (Fig. 7), with residual activity in the stromal fraction that may be due to some undetected thylakoid contamination. Nevertheless, the preprocessed enzyme may be partially active in the stroma. This analysis also revealed that the OAS-B protein is localized specifically to the chloroplastic stroma.

Comparison of the profiles of the proteins in the thylakoid lumen by 2-D electrophoresis for the wild type and *cs26* allowed for the identification of different proteins that dramatically decrease in abundance in the absence of CS26 in this compartment (Table V). For example, the peripheral thylakoid ATP synthase CF1 α- and β-subunits were strongly reduced in the *cs26* mutant. This defect was also observed in the *flu* mutant, showing high accumulations of ROS that significantly affected ATP synthase activity (Mahler et al., 2007). Furthermore, the HCF136 and Deg1 protein levels were very low in the *cs26* mutant, which are essential for the correct assembly and repair of PSII (Meurer et al., 1998; Kapri-Pardes et al., 2007). HCF136 has been described in cyanobacteria and plants as an essential protein for the biogenesis and assembly of PSII because of its stabilization of the newly synthesized D1 protein and its subsequent binding to a D2-cytochrome b_{559} precomplex (Plücken et al., 2002; Komenda et al., 2008). Similarly, Deg1 is involved in photoinhibition repair by degrading the PSII reaction center protein D1 (Kapri-Pardes et al., 2007). PSII repair is known to involve the partial disassembly of PSII, degradation of the damaged proteins, and incorporation and reassembly of the newly synthesized proteins (Nixon et al., 2010). Therefore, the reduction of HCF136 and Deg1 as well as other proteins, such as TLP38 and FKBP-type proteins, that are involved in

Table V. *Differential display of lumenal proteins from the cs26 mutant versus the wild type, analyzed by MALDI-TOF*

Identifications, functions, and fold changes of the different isolated spots are shown. Fold change is expressed as change in protein expression as calculated by PDQuest 2-D analysis software. The value 0 represents an absence of protein.

Spot	Protein Name	Accession No./Gene Locus NO.	Function	Fold Change
1	ATP synthase CF1 α-subunit (thylakoid membrane)	gi 7525018/ATCG00120	Hydrogen ion-transporting ATPase activity	0.004
2	ATP synthase CF1 β-subunit (thylakoid membrane)	gi 7525040/ATCG00480	Hydrogen ion transmembrane transporter activity	0
3	C-terminal processing protease	gi 15236628/AT4G17740	Ser-type peptidase activity/D1-processing protease	0
4	Cyclophilin/PPIase TLP38	gi 42564190/AT3G15520	Peptidyl-prolyl cis-trans-isomerase activity/immunophilin/protein folding	0.14
5, 6	HCF136 (high chlorophyll fluorescence136)	gi 15237225/AT5G23120	Stability and/or assembly factor of PSII	0.03/0
7	Deg1 protease	gi 2565436/AT3G27925	Trypsin-like Ser protease	0
8	LEAF FNR1 (stroma/thylakoid membrane)	gi145334919/AT5G66190	Ferredoxin:NADP(H) oxidoreductase/electron transporter	0
9, 10, 11	PSBO-1 (oxygen-evolving enhancer33)	gi 15240013/AT5G66570	Oxygen-evolving activity	0.76/0 to 1/0.04
12, 13	PSBO-2 (PSII subunit O-2)	gi 15230324/AT3G50820	Oxygen-evolving activity	0/0 to 1
14	PSII reaction center PsbP family protein	gi 79325123/AT4G15510	Calcium ion binding	0
15, 16	PSBP-1 (oxygen-evolving enhancer protein2)	gi 15222166/AT1G06680	Regulation of oxygen evolution	0 to 1/0
17	AAA-type ATPase family protein	gi 18398708/AT2G18330	ATPase activity	0
18	Immunophilin/FKBP-type PPIase	gi 15224305/AT2G43560	Peptidyl-prolyl cis-trans-isomerase activity/protein folding	0.01
19	Thylakoid lumenal 17.9-kD protein	gi 15234798/AT4G24930	Unknown	0.03
20	Thylakoid lumenal 17.4-kD protein	gi 30696347/AT5G53490	Unknown	0.01
21	Thylakoid lumenal 15-kD protein	gi 18406661/AT2G44920	Unknown	0
22	FIBRILLIN2; plastid-lipid-associated protein PAP (thylakoid membrane)	gi 15227428/AT2G35490	Structural molecule activity	111.68

the correct folding of lumenal proteins may strongly affect the assembly and repair of the photosynthetic machinery and therefore photosynthetic performance.

The comparative wild-type versus *cs26* lumenal proteomic analysis revealed only one significantly up-regulated protein in *cs26*. This protein is FIBRILLIN2, which belongs to the PAP/fibrilline-like family that is localized to the plastoglobules (Vidi et al., 2006; Lundquist et al., 2012). Curiously, it has been reported that the numbers of plastoglobules increase in plants that are subjected to environmental conditions that produce oxidative stress on the photosynthetic apparatus (Sam et al., 2003).

The mutant phenotype and the photosynthetic rates that are observed in *cs26* under LD but not SD are indicative of severe damage to the photosynthetic machinery by failure of the repair mechanisms of the photosystems during periods of prolonged exposure to light. In conclusion, when grown under low light intensity during LD, the *cs26* mutant behaves as it would if exposed to high irradiance.

As previously mentioned, a similar phenotype has been described in a null mutant of the *LTO1* gene that encodes for a lumen thioloxidoreductase that catalyzes the formation of disulfide bonds in the thylakoid lumen (Karamoko et al., 2011). This enzyme is required for the assembly of PSII through the formation of disulfide bonds in the PsbO subunit of the lumenal PSII oxygen-evolving complex (Karamoko et al., 2011). The metabolite *S*-sulfocysteine, which is synthesized inside of the lumen by CS26, may function in a similar manner by up-regulating the oxidation of the Cys residues of lumenal proteins whose activities are modified by these oxidation events (Buchanan and Luan, 2005), such as FKBP13, which interacts with the Rieske protein (Gopalan et al., 2004). Other target lumenal proteins of *S*-sulfocysteine include STN7 kinase, which is involved in LHCII, and CP29, which is

phosphorylated during photosynthetic acclimation and the high-light-induced disassembly of PSII complexes (Pesaresi et al., 2009; Fristedt and Vener, 2011). Since *S*-Cys may act chemically as an oxidative molecule by reacting with reduced thiols (Neta and Huie, 1985), the absence of the SSCS enzyme in the lumen may alter the redox regulation of proteins that are essential for maintaining the repair mechanisms of the photosystems, thereby causing plant light sensitivity in certain lighting conditions.

In conclusion, our studies suggest that the protein CS26, which is located in the thylakoid lumen, is essential for the proper photosynthetic performance of Arabidopsis chloroplasts, and consequently, the loss of CS26 has a dramatic impact on photosynthetic parameters, particularly under LD.

MATERIALS AND METHODS

Plant Materials and Growth Conditions

The Arabidopsis (*Arabidopsis thaliana*) wild-type ecotype Columbia, the SALK_034133 (*cs26*) and GABI_684B07 (*oas-b*) transferred DNA insertion mutant lines, and the complemented *cs26*:P35S-CS26 line were used in this work (Bermúdez et al., 2010). The plants were grown in soil under LD of 16 h of white light (120 μmol m^{-2} s^{-1}) at 22°C/8 h of dark at 20°C for 3 weeks or under SD of 8 h of white light (same intensity as above) at 22°C/16 h of dark at 20°C for 5 weeks.

LMA

LMA was measured for five fully expanded leaves from different individuals per line and calculated as the ratio of leaf dry weight to leaf area. Dry weights were determined after oven drying for 48 h at 60°C.

Gas-Exchange and Chlorophyll Fluorescence Measurements

Leaf gas exchange and chlorophyll *a* fluorescence were measured simultaneously with an open infrared gas-exchange analyzer system that was equipped with a leaf chamber fluorometer (Li-6400-40; Li-Cor). Environmental conditions in the leaf chamber consisted of a leaf-to-air vapor pressure deficit of 1.2 to 1.8 kPa and a leaf temperature of 22°C. The amount of blue light was set to 10% photosynthetic photon flux density (PPFD) to maximize stomatal aperture. Gas-exchange and chlorophyll fluorescence measurements included determinations of the net CO_2 assimilation rate and fluorescence parameters at varying PAR intensities (A_N-PAR curves) and substomatal CO_2 concentrations (A_N-C_i curves). Six A_N-PAR curves per line were obtained from different plants that were grown under the LD. The C_a within the leaf chamber was maintained at 400 μmol CO_2 mol^{-1} air. In the dark-adapted leaves, measurements were initiated at a PPFD of zero to obtain values for R_{dark}, $g_{s,dark}$, and F_v/F_m. For F_v/F_m, a measuring light of 0.5 μmol photon m^{-2} s^{-1} was set at a frequency of 600 Hz to determine the F_o. To obtain the maximum fluorescence (F_m), saturation pulses of 8,500 μmol photons m^{-2} s^{-1} for 0.8 s were applied. F_v/F_m was calculated as $(F_m - F_o)/F_m$. Thereafter, gas exchange and chlorophyll fluorescence were measured at increasing PAR intensities up to 2,000 μmol m^{-2} s^{-1}, with a total of 12 different intensities.

The actual quantum efficiency of PSII-driven electron transport (Φ_{PSII}) was determined according to Genty et al. (1989) as:

$$\Phi_{PSII} = \left(F_m{}' - F_s{}'\right)\big/F_m{}'$$

where $F_s{}'$ is the steady-state fluorescence of the light (PPFD of 1,000 μmol m^{-2} s^{-1}) and $F_m{}'$ is the maximum fluorescence in the light, which was obtained using a light-saturating pulse (8,500 μmol m^{-2} s^{-1}; Genty et al., 1989). Because Φ_{PSII} represents the number of electrons that are transferred per photon absorbed by PSII, *J* was calculated as:

$$J = \Phi_{PSII} \cdot PPED \cdot \alpha \cdot \beta$$

where α is the leaf absorbance and β is the distribution of absorbed energy between the two photosystems. The product of $\alpha \cdot \beta$ was determined from the relationship between Φ_{PSII} and the quantum efficiency of photosynthesis ($\phi CO_2 = A_N + R_L/PPFD$), which was obtained by varying the light intensity under nonphotorespiratory conditions in an atmosphere containing approximately 1% O_2 (Warren and Dreyer, 2006) in the wild-type and *cs26* mutant lines under the two photoperiods. The rate of nonphotorespiratory CO_2 evolution in the light (R_L) was assumed to be half of R_{dark} (Galmés et al., 2011). The product of $\alpha \cdot \beta$ was 0.365 ± 0.007 and 0.470 ± 0.013 for the wild type under LD and SD, respectively, whereas it was 0.267 ± 0.015 and 0.419 ± 0.019 for the *cs26* mutant under LD and SD, respectively.

Six A_N-C_i curves per line were obtained from different plants for each photoperiod. In the light-adapted leaves, photosynthesis was initiated at a C_a of 400 μmol mol^{-1} and a saturating PPFD of 1,000 μmol m^{-2} s^{-1} (the light saturation that was assessed by light-response curves was near 800 μmol m^{-2} s^{-1}). Once steady state was reached (typically after 20 min), C_a was decreased stepwise down to 50 μmol mol^{-1} air. Upon completion of the measurements at low C_a, it was returned to 400 μmol mol^{-1} air to restore the original A_N. Next, C_a was increased stepwise to 2,000 μmol mol^{-1} air. The A_N-C_i curves consisted of 11 different C_a values and were transformed to A_N-C_c curves as described below.

The g_m was estimated following the variable *J* method (Harley et al., 1992) as:

$$g_m = A_N/\left(C_i - \left(\Gamma^*(J + 8(A_N + R_L))\right)/(J - 4(A_N + R_L))\right)$$

The Rubisco specificity factor has not yet been published for Arabidopsis; hence, the chloroplast CO_2 compensation point (Γ^*) was obtained as a proxy of the substomatal CO_2 compensation point in the absence of mitochondrial respiration (C_i^*), which was estimated according to the method of Laisk as described (Galmés et al., 2006). Because values for the Rubisco specificity factor, and hence Γ^*, depend upon the amino acid compositions of Rubisco subunits, they do not differ between lines of the same species. Therefore, only wild-type plants were used to estimate Γ^*. At 22°C, a C_i^* value of 41.2 ± 2.6 mmol CO_2 mol^{-1} air was obtained ($n = 4$). Applying the temperature dependence functions that were described by Bernacchi et al. (2002) resulted in a C_i^* of 48.4 ± 2.6 at 25°C, which was similar to previously reported values (Flexas et al., 2007a).

Estimated g_m values were used to convert the A_N-C_i curves into A_N-C_c curves. $V_{c,max}$ and J_{max} were then calculated from the A_N-C_c curves (Flexas et al., 2007a). With the exception of Γ^*, the kinetic parameters of Rubisco and its temperature dependence were taken from a previous report (Bernacchi et al., 2001).

Corrections for the leakage of CO_2 into and out of the leaf chamber of the Li-6400 were applied to all gas-exchange data (Flexas et al., 2007b).

Chlorophyll Fluorescence Imaging

Chlorophyll fluorescence parameters were measured using a FluorImager chlorophyll fluorescence imaging system (Technologica). The method applied involved preprogrammed treatments of 30-min dark periods to determine F_v/F_m, for which F_m was obtained at saturation pulses of approximately 5,600 μmol photon m^{-2} s^{-1}. Actinic growth light (150 μmol m^{-2} s^{-1}) and saturating light (800 μmol m^{-2} s^{-1}) exposure times and saturating light pulses were applied to obtain the following parameters: F_v/F_m, Φ_{PSII}, $F_v{}'/F_m{}'$ (where $F_v{}'$ is equal to $F_m - F_o{}'$, and $F_o{}'$ is the minimal fluorescence level of light at which the primary/secondary electron-accepting plastoquinone of PSII is maximally oxidized), NPQ [which is calculated from $(F_m/F_m{}') - 1$], and qP (or $F_q{}'/F_v{}'$). Three values at each actinic light intensity for three replicates per line were obtained for both photoperiods. The calculations and imaging of the parameters were performed automatically using the FluorImager software. qL, defined as the fraction of open PSII centers, was calculated post measurement from the images of $F_q{}'/F_m{}'$, $F_o{}'$, and $F_s{}'$, given by $(F_q{}'/F_m{}')/(F_o{}'/F_s{}')$ (Baker, 2008).

Quantification of Rubisco Protein

Leaves from plants that were grown under both photoperiods were ground in 50 mM Tris-HCl (pH 7.5), the extract was centrifuged at 7,500g for 15 min, and the total soluble protein level was determined in the supernatant according to the method of Bradford (1976). The protein aliquots (5 μg) and

pure Rubisco were subject to SDS-PAGE using 12% (w/v) polyacrylamide gels and Coomassie Brilliant Blue staining. The Rubisco titration was performed by quantification with Quantity One software (Bio-Rad) using known concentrations of purified Rubisco from Arabidopsis.

RNA Isolation and *CS26* Expression by Real-Time Reverse Transcription-PCR Analysis

The RNA isolation and real-time PCR analysis of the expression of the *CS26* gene were performed at different stages of development in wild-type plants, according to the growth stages described by Boyes et al. (2001). At each developmental stage, total RNA from rosette leaves, stems, and flowers at developmental stage 6.1 were extracted and analyzed. Real-time reverse transcription-PCR analyses were performed as described previously (Bermúdez et al., 2010).

Assay of Enzymatic Activity

SSCS activity was measured as described previously (Bermúdez et al., 2010).

Isolation of Stromal and Thylakoid Lumenal Contents, and Immunoblot Analyses

Enriched chloroplast preparations from Arabidopsis were obtained from 40 g of leaves, and stromal and lumenal protein extracts were isolated as described previously (Kieselbach et al., 1998).

Analyses of the protein fractions were performed in duplicate, in which one replicate was stained with Coomassie blue and the other was used for the immunoblot analyses. For the latter analyses, 100 μg of stromal protein or 30 μg of lumenal protein extracts was electrophoresed on 12% acrylamide gels before transfer to polyvinylidene difluoride membranes (Immun-Blot PVDF; Bio-Rad) according to the manufacturer's instructions. The custom-made polyclonal anti-recombinant CS26 antibody (Biomedal) and secondary antibodies were diluted 1:30,000 and 1:10,000, respectively, in phosphate-buffered saline containing 0.1% Tween 20 (Sigma-Aldrich) and 5% (w/v) milk powder. Anti-Rubisco activase and anti-PsbO antibodies were used as markers of cross-contamination between the stromal and lumenal extracts, respectively. The ECL Advance Immunoblotting Detection System (GE Healthcare) was used to detect the proteins with horseradish peroxidase-conjugated anti-rabbit secondary antibodies.

Two-Dimensional Electrophoresis

The lumenal proteins (100 μg) were separated by isoelectric focusing in the first dimension and by SDS-PAGE in the second dimension according to Schubert et al. (2002), with the following modifications: the lumenal proteins were solubilized in 8 M urea, 2% (w/v) CHAPS, 50 mM dithiothreitol, 0.2% (v/v) ampholytes (Bio-Lyte 3-10 buffer; Bio-Rad), and a trace of bromophenol blue and applied during rehydration to a linear immobilized pH gradient strip, pH 4 to 7.

Isoelectric focusing was performed at 22°C in the Protean IEF Cell (Bio-Rad) in three steps: (1) 250 V for 15 min; (2) 10,000 V for 1 h; (3) 10,000 V up to 40,000 V. Intensity was fixed to a 50-μA per immobilized pH gradient strip to avoid overheating the system.

Prior to the second dimension, the gel strips were equilibrated for 2 × 15 min in a solution containing 6 M urea, 20% (v/v) glycerol, 2% (w/v) SDS, and 0.4 M Tris-HCl, pH 8.8, with 50 mM dithiothreitol added to the first equilibration solution and 2.5% (w/v) iodoacetamide added to the second. The gel strips were washed with a solution containing 25 mM Tris-HCl, pH 8.3, 0.2 M Gly, and 0.1% SDS (w/v).

The equilibrated gel strips were placed on top of vertical polyacrylamide gels (12% acrylamide and SDS; Laemmli, 1970). A denaturing solution (0.5% [w/v] low-melting-point agarose, 0.1% [w/v] SDS, 0.25 M Tris-HCl, 0.2 M Gly, and a trace of bromophenol blue) was loaded on the gel strips. Electrophoresis was carried out at 240 V and 35 mA per gel for 5 h using the Protean II xi Cell (Bio-Rad).

The gels were stained with silver nitrate using the Silver Staining Kit, Protein (GE Healthcare) according to the manufacturer's instructions. The two-dimensional silver-stained gels were scanned with a GS-800 Densitometer (Bio-Rad). Image analysis was conducted with PDQuest 8.0 2-D analysis software (Bio-Rad).

Protein Identification by Mass Spectrometry

Spots of interest were excised from the stained one-dimensional or 2-D gels using an ExQuest Spot Cutter System (Bio-Rad). The stain was eliminated by incubation of the bands with acetonitrile for 10 min and vacuum drying for 15 min. The spots were digested by 0.013 μg μL^{-1} trypsin and 50 mM NH$_4$HCO$_3$, pH 7.8. After incubation for 30 min at 4°C, the supernatant was removed, and 10 μM of 50 mM NH$_4$HCO$_3$, pH 7.8, was added and incubated for 15 h at 37°C. The reaction was stopped by the addition of 0.5% (v/v) TCA. After digestion, the peptide mass fingerprint data were collected by MALDI-mass spectrometry analysis on an Autoflex MALDI-TOF mass spectrometer (Bruker Daltonics). Before each analysis, the instrument was externally calibrated using the Peptide Calibration Standard (Bruker Daltonics). Proteins were identified according to the highest ranked result by searching the National Center for Biotechnology Information nonredundant protein sequence database using the MASCOT search engine (Matrix Science). Searching parameters included the carbamidomethylation of Cys and Met oxidation.

Statistical Analysis

A univariate ANOVA was performed to reveal the differences between genotypes and photoperiods for the studied parameters. The analyses were performed using the Origin Pro 7.5 software package (Originlab). Comparisons were tested using Duncan analysis at a significance level of $P < 0.05$. When possible, a significance level of $P < 0.01$ was applied. If required, multiple comparison tests were used by the application of Duncan's multiple range test at a significance level of $P < 0.05$ (or $P < 0.01$) for the analysis of mean differences using Statgraphics Centurion (Statpoint Technologies).

Sequence data from this article can be found in the GenBank/EMBL data libraries under accession numbers CS26 (At3g03630), OAS-B (At2g43750), CS26 T-DNA mutant (SALK_034133), and OAS-B T-DNA mutants (GABI_684B07).

Supplemental Data

The following materials are available in the online version of this article.

Supplemental Figure S1. Cross-contamination between stromal and lumenal fractions.

Supplemental Figure S2. Proteome map of the chloroplast lumen of the wild type and the mutant *cs26*.

Supplemental Table S1. Photosynthetic characterization of wild-type, *cs26*, and *cs26*:P35S-CS26 plants grown under LD.

Supplemental Table S2. Photosynthetic parameters derived from light-response curves in wild-type, *cs26*, and *cs26*:P35S-CS26 plants under LD.

LITERATURE CITED

Aldridge C, Cain P, Robinson C (2009) Protein transport in organelles: protein transport into and across the thylakoid membrane. FEBS J **276:** 1177–1186

Alvarez C, Lozano-Juste J, Romero LC, García I, Gotor C, León J (2011) Inhibition of Arabidopsis O-acetylserine(thiol)lyase A1 by tyrosine nitration. J Biol Chem **286:** 578–586

Asada K (1999) The water-water cycle in chloroplasts: scavenging of active oxygens and dissipation of excess photons. Annu Rev Plant Physiol Plant Mol Biol **50:** 601–639

Baker NR (2008) Chlorophyll fluorescence: a probe of photosynthesis in vivo. Annu Rev Plant Biol **59:** 89–113

Bermúdez MA, Páez-Ochoa MA, Gotor C, Romero LC (2010) *Arabidopsis S*-sulfocysteine synthase activity is essential for chloroplast function and long-day light-dependent redox control. Plant Cell **22:** 403–416

Bernacchi C, Singsaas E, Pimentel C, Portis A Jr, Long S (2001) Improved temperature response functions for models of Rubisco limited photosynthesis. Plant Cell Environ **24:** 253–259

Bernacchi CJ, Portis AR, Nakano H, von Caemmerer S, Long SP (2002) Temperature response of mesophyll conductance: implications for the determination of Rubisco enzyme kinetics and for limitations to photosynthesis in vivo. Plant Physiol **130:** 1992–1998

Bondarava N, Gross CM, Mubarakshina M, Golecki JR, Johnson GN, Krieger-Liszkay A (2010) Putative function of cytochrome b559 as a plastoquinol oxidase. Physiol Plant **138:** 463–473

Boyes DC, Zayed AM, Ascenzi R, McCaskill AJ, Hoffman NE, Davis KR, Görlach J (2001) Growth stage-based phenotypic analysis of *Arabidopsis*: a model for high throughput functional genomics in plants. Plant Cell **13:** 1499–1510

Bradford MM (1976) A rapid and sensitive method for the quantitation of microgram quantities of protein utilizing the principle of protein-dye binding. Anal Biochem **72:** 248–254

Buchanan BB, Luan S (2005) Redox regulation in the chloroplast thylakoid lumen: a new frontier in photosynthesis research. J Exp Bot **56:** 1439–1447

Douce R, Neuburger M (1999) Biochemical dissection of photorespiration. Curr Opin Plant Biol **2:** 214–222

Droux M, Ruffet ML, Douce R, Job D (1998) Interactions between serine acetyltransferase and O-acetylserine (thiol) lyase in higher plants: structural and kinetic properties of the free and bound enzymes. Eur J Biochem **255:** 235–245

Ekelund NG (2000) Interactions between photosynthesis and 'light-enhanced dark respiration' (LEDR) in the flagellate Euglena gracilis after irradiation with ultraviolet radiation. J Photochem Photobiol B **55:** 63–69

Flexas J, Díaz-Espejo A, Berry JA, Cifre J, Galmés J, Kaldenhoff R, Medrano H, Ribas-Carbó M (2007a) Analysis of leakage in IRGA's leaf chambers of open gas exchange systems: quantification and its effects in photosynthesis parameterization. J Exp Bot **58:** 1533–1543

Flexas J, Diaz-Espejo A, Galmés J, Kaldenhoff R, Medrano H, Ribas-Carbo M (2007b) Rapid variations of mesophyll conductance in response to changes in CO_2 concentration around leaves. Plant Cell Environ **30:** 1284–1298

Fristedt R, Vener AV (2011) High light induced disassembly of photosystem II supercomplexes in Arabidopsis requires STN7-dependent phosphorylation of CP29. PLoS ONE **6:** e24565

Galmés J, Conesa MÀ, Ochogavía JM, Perdomo JA, Francis DM, Ribas-Carbó M, Savé R, Flexas J, Medrano H, Cifre J (2011) Physiological and morphological adaptations in relation to water use efficiency in Mediterranean accessions of Solanum lycopersicum. Plant Cell Environ **34:** 245–260

Galmés J, Medrano H, Flexas J (2006) Acclimation of Rubisco specificity factor to drought in tobacco: discrepancies between in vitro and in vivo estimations. J Exp Bot **57:** 3659–3667

Genty B, Briantais JM, Baker NR (1989) The relationship between the quantum yield of photosynthetic electron transport and quenching of chlorophyll fluorescence. Biochim Biophys Acta **990:** 87–179

Gilbert GH, Antonson DE, Mjor IA, Ringelberg ML, Dolan TA, Foerster U, Legler DW, Heft MW, Duncan RP (1996) Coronal caries, root fragments, and restoration and cusp fractures in US adults. Caries Res **30:** 101–111

Gopalan G, He Z, Balmer Y, Romano P, Gupta R, Héroux A, Buchanan BB, Swaminathan K, Luan S (2004) Structural analysis uncovers a role for redox in regulating FKBP13, an immunophilin of the chloroplast thylakoid lumen. Proc Natl Acad Sci USA **101:** 13945–13950

Gutensohn K, Magens M, Krüger W, Kröger N, Kühnl P (2006) Comparison of flow cytometry vs. a haematology cell analyser-based method to guide the optimal time-point for peripheral blood stem cell apheresis. Vox Sang **90:** 53–58

Harley PC, Loreto F, Di Marco G, Sharkey TD (1992) Theoretical considerations when estimating the mesophyll conductance to CO_2 flux by analysis of the response of photosynthesis to CO_2. Plant Physiol **98:** 1429–1436

Horton P, Ruban AV, Walters RG (1996) Regulation of light harvesting in green plants. Annu Rev Plant Physiol Plant Mol Biol **47:** 655–684

Howarth JR, Domínguez-Solís JR, Gutiérrez-Alcalá G, Wray JL, Romero LC, Gotor C (2003) The serine acetyltransferase gene family in Arabidopsis thaliana and the regulation of its expression by cadmium. Plant Mol Biol **51:** 589–598

Kapri-Pardes E, Naveh L, Adam Z (2007) The thylakoid lumen protease Deg1 is involved in the repair of photosystem II from photoinhibition in *Arabidopsis*. Plant Cell **19:** 1039–1047

Karamoko M, Cline S, Redding K, Ruiz N, Hamel PP (2011) Lumen Thiol Oxidoreductase1, a disulfide bond-forming catalyst, is required for the assembly of photosystem II in *Arabidopsis*. Plant Cell **23:** 4462–4475

Kidner C, Sundaresan V, Roberts K, Dolan L (2000) Clonal analysis of the Arabidopsis root confirms that position, not lineage, determines cell fate. Planta **211:** 191–199

Kieselbach T, Hagman , Andersson B, Schröder WP (1998) The thylakoid lumen of chloroplasts: isolation and characterization. J Biol Chem **273:** 6710–6716

Kim CM, Park SH, Je BI, Park SH, Park SJ, Piao HL, Eun MY, Dolan L, Han CD (2007) *OsCSLD1*, a cellulose synthase-like D1 gene, is required for root hair morphogenesis in rice. Plant Physiol **143:** 1220–1230

Kim YX, Steudle E (2007) Light and turgor affect the water permeability (aquaporins) of parenchyma cells in the midrib of leaves of Zea mays. J Exp Bot **58:** 4119–4129

Komenda J, Nickelsen J, Tichý M, Prásil O, Eichacker LA, Nixon PJ (2008) The cyanobacterial homologue of HCF136/YCF48 is a component of an early photosystem II assembly complex and is important for both the efficient assembly and repair of photosystem II in Synechocystis sp. PCC 6803. J Biol Chem **283:** 22390–22399

Koussevitzky S, Nott A, Mockler TC, Hong F, Sachetto-Martins G, Surpin M, Lim J, Mittler R, Chory J (2007) Signals from chloroplasts converge to regulate nuclear gene expression. Science **316:** 715–719

Laemmli UK (1970) Cleavage of structural proteins during the assembly of the head of bacteriophage T4. Nature **227:** 680–685

Lepistö A, Kangasjärvi S, Luomala E-M, Brader G, Sipari N, Keränen M, Keinänen M, Rintamäki E (2009) Chloroplast NADPH-thioredoxin reductase interacts with photoperiodic development in Arabidopsis. Plant Physiol **149:** 1261–1276

Loreto F, Tsonev T, Centritto M (2009) The impact of blue light on leaf mesophyll conductance. J Exp Bot **60:** 2283–2290

Lundquist PK, Poliakov A, Bhuiyan NH, Zybailov B, Sun Q, van Wijk KJ (2012) The functional network of the Arabidopsis plastoglobule proteome based on quantitative proteomics and genome-wide coexpression analysis. Plant Physiol **158:** 1172–1192

Mahler H, Wuennenberg P, Linder M, Przybyla D, Zoerb C, Landgraf F, Forreiter C (2007) Singlet oxygen affects the activity of the thylakoid ATP synthase and has a strong impact on its gamma subunit. Planta **225:** 1073–1083

Meurer J, Plücken H, Kowallik KV, Westhoff P (1998) A nuclear-encoded protein of prokaryotic origin is essential for the stability of photosystem II in Arabidopsis thaliana. EMBO J **17:** 5286–5297

Moskvin OV, Ivanov BN, Ignatova LK, Kollmeier MA (2000) Light-induced stimulation of carbonic anhydrase activity in pea thylakoids. FEBS Lett **470:** 375–377

Mühlenbock P, Szechynska-Hebda M, Plaszczyca M, Baudo M, Mateo A, Mullineaux PM, Parker JE, Karpinska B, Karpinski S (2008) Chloroplast signaling and LESION SIMULATING DISEASE1 regulate crosstalk between light acclimation and immunity in *Arabidopsis*. Plant Cell **20:** 2339–2356

Müller P, Li XP, Niyogi KK (2001) Non-photochemical quenching: a response to excess light energy. Plant Physiol **125:** 1558–1566

Murakami R, Ifuku K, Takabayashi A, Shikanai T, Endo T, Sato F (2002) Characterization of an Arabidopsis thaliana mutant with impaired psbO, one of two genes encoding extrinsic 33-kDa proteins in photosystem II. FEBS Lett **523:** 138–142

Neta P, Huie RE (1985) Free-radical chemistry of sulfite. Environ Health Perspect **64:** 209–217

Nixon PJ, Michoux F, Yu J, Boehm M, Komenda J (2010) Recent advances in understanding the assembly and repair of photosystem II. Ann Bot (Lond) **106:** 1–16

Padmasree K, Padmavathi L, Raghavendra AS (2002) Essentiality of mitochondrial oxidative metabolism for photosynthesis: optimization of carbon assimilation and protection against photoinhibition. Crit Rev Biochem Mol Biol **37:** 71–119

Peltier JB, Emanuelsson O, Kalume DE, Ytterberg J, Friso G, Rudella A, Liberles DA, Söderberg L, Roepstorff P, von Heijne G, et al (2002) Central functions of the lumenal and peripheral thylakoid proteome of *Arabidopsis* determined by experimentation and genome-wide prediction. Plant Cell **14**: 211–236

Pesaresi P, Hertle A, Pribil M, Kleine T, Wagner R, Strissel H, Ihnatowicz A, Bonardi V, Scharfenberg M, Schneider A, et al (2009) *Arabidopsis* STN7 kinase provides a link between short- and long-term photosynthetic acclimation. Plant Cell **21**: 2402–2423

Plücken H, Müller B, Grohmann D, Westhoff P, Eichacker LA (2002) The HCF136 protein is essential for assembly of the photosystem II reaction center in Arabidopsis thaliana. FEBS Lett **532**: 85–90

Pogson BJ, Woo NS, Förster B, Small ID (2008) Plastid signalling to the nucleus and beyond. Trends Plant Sci **13**: 602–609

Raghavendra AS, Padmasree K (2003) Beneficial interactions of mitochondrial metabolism with photosynthetic carbon assimilation. Trends Plant Sci **8**: 546–553

Reddy MM, Vani T, Raghavendra AS (1991) Light-enhanced dark respiration in mesophyll protoplasts from leaves of pea. Plant Physiol **96**: 1368–1371

Robinson C, Thompson SJ, Woolhead C (2001) Multiple pathways used for the targeting of thylakoid proteins in chloroplasts. Traffic **2**: 245–251

Sam O, Ramírez C, Coronado MJ, Testillano PS, Risueño MC (2003) Changes in tomato leaves induced by NaCl stress: leaf organization and cell ultrastructure. Biol Plant **47**: 361–366

Saradadevi K, Raghavendra AS (1992) Dark respiration protects photosynthesis against photoinhibition in mesophyll protoplasts of pea (*Pisum sativum*). Plant Physiol **99**: 1232–1237

Schubert M, Petersson UA, Haas BJ, Funk C, Schröder WP, Kieselbach T (2002) Proteome map of the chloroplast lumen of Arabidopsis thaliana. J Biol Chem **277**: 8354–8365

Singh KK, Shyam R, Sane PV (1996) Reactivation of photosynthesis in the photoinhibited green alga Chlamydomonas reinhardtii: role of dark respiration and of light. Photosynth Res **49**: 11–31

Stessman D, Miller A, Spalding M, Rodermel S (2002) Regulation of photosynthesis during Arabidopsis leaf development in continuous light. Photosynth Res **72**: 27–37

Vidi P-A, Kanwischer M, Baginsky S, Austin JR, Csucs G, Dörmann P, Kessler F, Bréhélin C (2006) Tocopherol cyclase (VTE1) localization and vitamin E accumulation in chloroplast plastoglobule lipoprotein particles. J Biol Chem **281**: 11225–11234

Warren CR, Dreyer E (2006) Temperature response of photosynthesis and internal conductance to CO_2: results from two independent approaches. J Exp Bot **57**: 3057–3067

Watanabe M, Kusano M, Oikawa A, Fukushima A, Noji M, Saito K (2008) Physiological roles of the β-substituted alanine synthase gene family in Arabidopsis. Plant Physiol **146**: 310–320

Wirtz M, Droux M, Hell R (2004) O-Acetylserine (thiol) lyase: an enigmatic enzyme of plant cysteine biosynthesis revisited in Arabidopsis thaliana. J Exp Bot **55**: 1785–1798

Wirtz M, Heeg C, Samami AA, Ruppert T, Hell R (2010) Enzymes of cysteine synthesis show extensive and conserved modification patterns that include N(α)-terminal acetylation. Amino Acids **39**: 1077–1086

Wirtz M, Hell R (2006) Functional analysis of the cysteine synthase protein complex from plants: structural, biochemical and regulatory properties. J Plant Physiol **163**: 273–286

Yoshida K, Watanabe C, Kato Y, Sakamoto W, Noguchi K (2008) Influence of chloroplastic photo-oxidative stress on mitochondrial alternative oxidase capacity and respiratory properties: a case study with Arabidopsis yellow variegated 2. Plant Cell Physiol **49**: 592–603

Zell MB, Fahnenstich H, Maier A, Saigo M, Voznesenskaya EV, Edwards GE, Andreo C, Schleifenbaum F, Zell C, Drincovich MF, et al (2010) Analysis of Arabidopsis with highly reduced levels of malate and fumarate sheds light on the role of these organic acids as storage carbon molecules. Plant Physiol **152**: 1251–1262

Zhang N, Kallis RP, Ewy RG, Portis AR Jr (2002) Light modulation of Rubisco in Arabidopsis requires a capacity for redox regulation of the larger Rubisco activase isoform. Proc Natl Acad Sci USA **99**: 3330–3334

Zybailov B, Rutschow H, Friso G, Rudella A, Emanuelsson O, Sun Q, van Wijk KJ (2008) Sorting signals, N-terminal modifications and abundance of the chloroplast proteome. PLoS ONE **3**: e1994
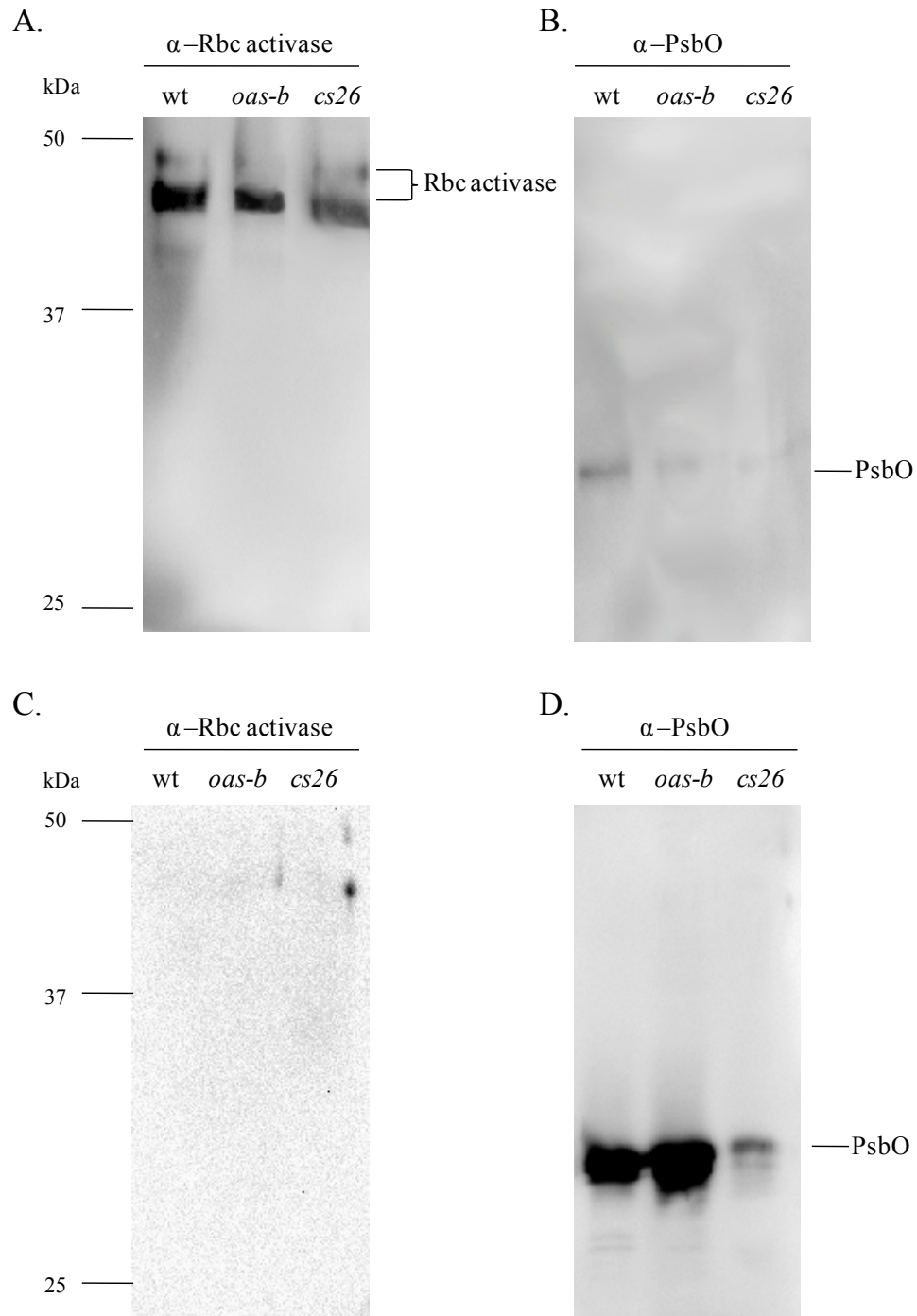
Supplemental Figure S1. Cross-contamination between stromal and lumenal fraction. Stromal and lumenal preparations from *Arabidopsis* were isolated from 40 g of leaves from wild type and *oas-b* and *cs26* mutant plants. To avoid signal saturation of Rubisco activase protein in the stromal extract, only 0.6 μg of stromal protein extracts, A-B, were loaded, and from the lumenal extract, 30 μg of protein, C-D, were loaded. All samples were electrophoresed on 12 % acrylamide gels and used for immunoblot analyses using anti-Rbc activase and anti-PsbO antibodies. A, In the stromal fraction, two bands at 47 and 42 kDa, corresponding with Rubisco activase were observed in all lines with the α-Rbc activase antibody. B, Weak band at 33 kDa corresponding with PsbO was also detected in the stromal extract when α-PsbO was used. There was no signal detection when α-Rbc activase was used in the lumenal extracts.
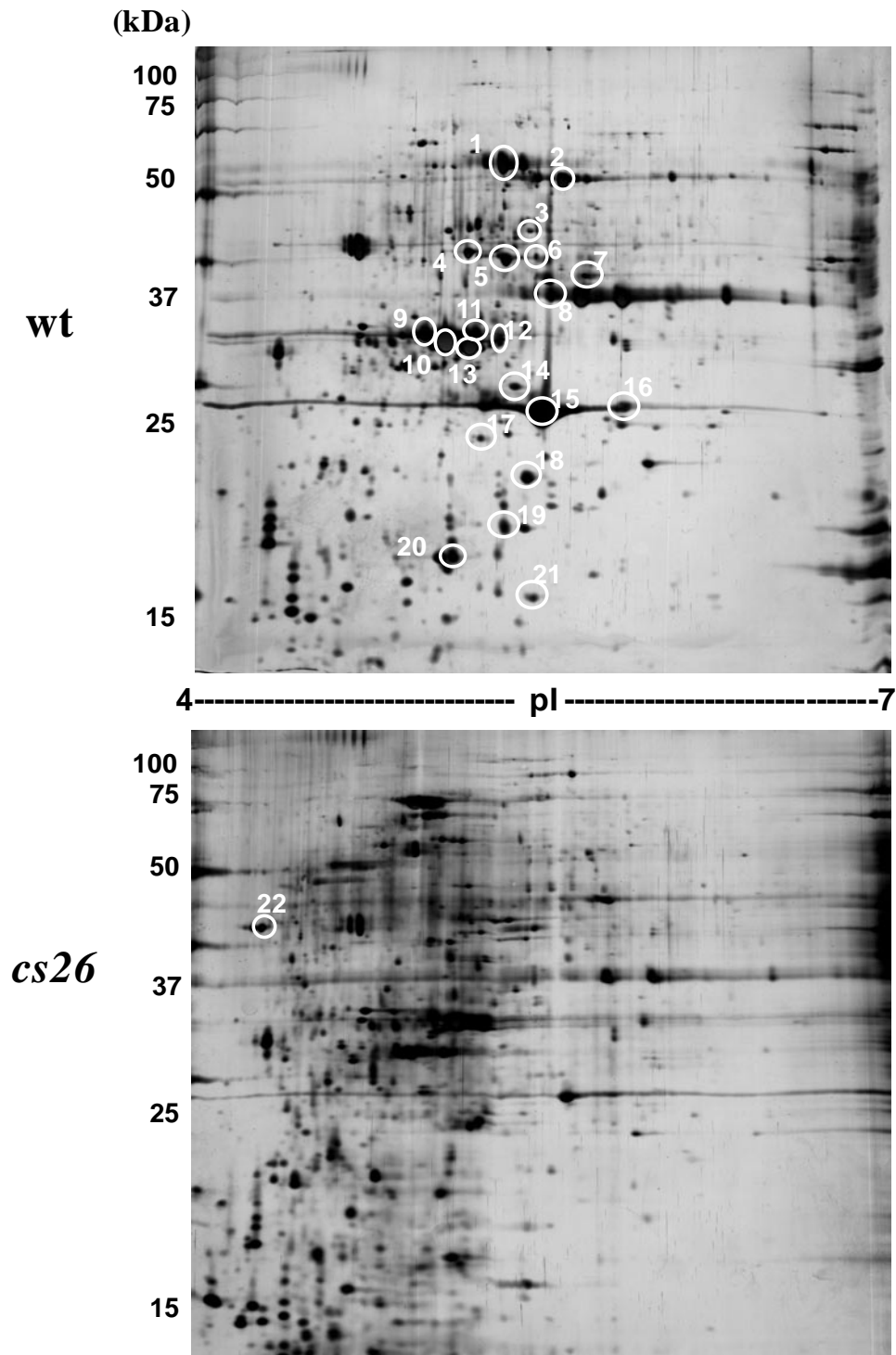
Supplemental Figure S2. Proteome map of the chloroplast lumen of the wild type and mutant *cs26*.

Silver-stained two-dimensional gels of 100 mg soluble lumenal proteins from the chloroplasts of 4-week-old plants that were grown in long-day conditions are shown. The proteins were resolved by SDS electrophoresis in a 12% polyacrylamide gel subsequent to isoelectrofocusing in a linear immobilised pH gradient from pH 4 to 7. The circles denote protein spot differences that were identified by MALDI-TOF. See Table V for detailed information on each identified protein.

Supplemental Table SI. Photosynthetic characterisation of wild-type, *cs26* and *cs26*:P35S-CS26 plants grown under long-day photoperiod

Net CO_2 assimilation rate (A_N), stomatal conductance (g_s), intrinsic water-use efficiency (A_N/g_s), mesophyll conductance (g_m), ratio of mesophyll and stomatal conductances to CO_2 (g_m/g_s), CO_2 concentration at the site of carboxylation (C_c), CO_2 compensation point on a C_c-basis (Γ_{Cc}), maximum velocity of carboxylation ($V_{c,max}$), maximum capacity of electron transport (J_{max}), ratio between maximum rates of electron transport and carboxylation ($J_{max}/V_{c,max}$), and mitochondrial respiration (R_{dark}) and g_s at darkness ($g_{s,dark}$) are shown. Values represent means ± SD (n = 6). A_N, g_s, A_N/g_s, g_m, g_m/g_s and C_c were obtained from steady-state measurements at a PAR of 1000 μmol m^{-2} s^{-1} and C_a of 400 μmol mol^{-1}. The g_m and C_c values were estimated according to the variable J method and used to convert the A_N-C_i curves into A_N-C_c. Γ_{Cc_based}, $V_{c,max}$ and J_{max} were taken from the A_N-C_c curves. R_{dark} and $g_{s,dark}$ were obtained from measurements at darkness and a C_a of 400 μmol mol^{-1}. An asterisk indicates significant differences at $P < 0.05$ between wild-type and mutant lines.

	wild-type	cs26	cs26:P35S-CS26
A_N (μmol CO_2 m^{-2} s^{-1})	8.3 ± 0.3	1.9 ± 0.3 *	7.9 ± 2.1
g_s (mol H_2O m^{-2} s^{-1})	0.20 ± 0.07	0.18 ± 0.08	0.19 ± 0.01
A_N/g_s (μmol CO_2 mol^{-1} H_2O)	41.4 ± 0.8	10.4 ± 0.5 *	42.5 ± 1.0
g_m (mol CO_2 m^{-2} s^{-1})	0.42 ± 0.09	0.01 ± 0.01 *	0.45 ± 0.07
g_m/g_s (mol CO_2 mol^{-1} H_2O)	2.05 ± 0.06	0.05 ± 0.01 *	2.30 ± 0.20
C_c (μmol CO_2 mol^{-1} air)	374 ± 34	340 ± 20	331 ± 23
R_{dark} (μmol CO_2 m^{-2} s^{-1})	-1.01 ± 0.25	-1.77 ± 0.33 *	-1.09 ± 0.20
$g_{s.dark}$ (mol H_2O m^{-2} s^{-1})	0.27 ± 0.13	0.28 ± 0.06	0.16 ± 0.10
$V_{c,max}$ (μmol CO_2 m^{-2} s^{-1})	24.6 ± 2.6	9.0 ± 2.3 *	22.2 ± 4.1
J_{max} (μmol CO_2 m^{-2} s^{-1})	48.6 ± 2.5	17.3 ± 5.1 *	49.4 ± 3.1
$J_{max}/V_{c,max}$	2.0 ± 0.2	1.9 ± 0.4	2.2 ± 0.3
Γ_{Cc} (μmol CO_2 mol^{-1} air)	51.0 ± 2.6	119.0 ± 10.0 *	50.6 ± 2.2

Supplemental Table SII. Photosynthetic parameters derived from light response curves in wild-type, *cs26* and *cs26*:P35S-CS26 plants under long-day photoperiod

J, electron transport rate; A_G, gross CO_2 assimilation rate (sum of net CO_2 assimilation rate (A_N) and light respiration (R_L)); PAR_{abs}, absorbed photosynthetic active radiation; NPQ, non-photochemical quenching are shown. J, J/A_G, NPQ and PAR_{abs}/J values were obtained at saturating light intensities (1000 μmol m^{-2} s^{-1}). PAR_{abs} was obtained by correcting the incoming PAR intensities with the leaf absorbance, taken from the α·β product and considering β constant and equal to 0.5. The values are averages ± SE for 6 replicates per genotype. An asterisk indicates significant differences at $P < 0.05$ between wild-type and the mutant lines.

	wild-type	*cs26*	*cs26*:P35S-CS26
J (μmol e$^-$ m^{-2} s^{-1})	50.1 ± 2.7	11.9 ± 2.7*	55.8 ± 5.2
Inflection point (μmol m^{-2} s^{-1})	533 ± 25	234 ± 56*	503 ± 37
Light compensation point (μmol m^{-2} s^{-1})	15.4 ± 6.6	51.3 ± 7.2*	8.2 ± 2.7
1/Quantum yield (mol hv mol^{-1} CO_2)	16.3 ± 1.1	23.6 ± 1.4*	16.0 ± 0.1
PAR_{abs}/J (mol hv mol^{-1} e$^-$)	3.5 ± 0.1	7.8 ± 0.9*	3.2 ± 0.2
J/A_G (mol e$^-$ mol^{-1} CO_2)	5.8 ± 0.5	8.3 ± 0.9*	5.9 ± 0.5
NPQ	0.9 ± 0.2	1.9 ± 0.5*	1.4 ± 0.4